ASTRONOMY & ASTROPHYSICS
SUPPLEMENT SERIES

Astron. Astrophys. Suppl. Ser. **143**, 145–179 (2000)

The first COMPTEL source catalogue

V. Schönfelder[1], K. Bennett[4], J.J. Blom[2], H. Bloemen[2], W. Collmar[1], A. Connors[3], R. Diehl[1], W. Hermsen[2], A. Iyudin[1], R.M. Kippen[3], J. Knödlseder[5], L. Kuiper[2], G.G. Lichti[1], M. McConnell[3], D. Morris[3], R. Much[4], U. Oberlack[1], J. Ryan[3], G. Stacy[3], H. Steinle[1], A. Strong[1], R. Suleiman[3], R. van Dijk[4], M. Varendorff[1], C. Winkler[4], and O.R. Williams[4]

[1] Max-Planck-Institut für extraterrestrische Physik, D-85740 Garching, Germany
[2] SRON–Utrecht, Sorbonnelaan 2, NL-3584 CA Utrecht, The Netherlands
[3] Space Science Center, University of New Hampshire, Durham, NH 03824-3525, U.S.A.
[4] Astrophysics Division, ESTEC, NL-2200 AG Noordwijk, The Netherlands
[5] Centre d'Étude Spatiale des Rayonnements (CESR), BP. 4346, F-31029 Toulouse Cedex, France

Received July 28; accepted December 20, 1999

Abstract. The imaging Compton telescope COMPTEL aboard NASA's Compton Gamma-Ray Observatory has opened the MeV gamma-ray band as a new window to astronomy. COMPTEL provided the first complete all-sky survey in the energy range 0.75 to 30 MeV. The catalogue, presented here, is largely restricted to published results. It contains firm as well as marginal detections of continuum and line emitting sources and presents upper limits for various types of objects. The numbers of the most significant detections are 32 for steady sources and 31 for gamma-ray bursters. Among the continuum sources, detected so far, are spin-down pulsars, stellar black-hole candidates, supernova remnants, interstellar clouds, nuclei of active galaxies, gamma-ray bursters, and the Sun during solar flares. Line detections have been made in the light of the 1.809 MeV ^{26}Al line, the 1.157 MeV ^{44}Ti line, the 847 and 1238 keV ^{56}Co lines, and the neutron capture line at 2.223 MeV. For the identification of galactic sources, a modelling of the diffuse galactic emission is essential. Such a modelling at this time does not yet exist at the required degree of accuracy. Therefore, a second COMPTEL source catalogue will be produced after a detailed and accurate modelling of the diffuse interstellar emission has become possible.

Key words: gamma rays: observations — catalogs — surveys

Send offprint requests to:
V. Schönfelder, e-mail: vos@mpe.mpg.de

1. Introduction

COMPTEL has demonstrated that the sky is rich in phenomena that can be studied at MeV energies. A variety of gamma-ray emitting objects are visible either in continuum or line emission. Among the continuum sources are spin-down pulsars, stellar black-hole candidates, supernova remnants, interstellar clouds, nuclei of active galaxies, gamma-ray bursters, and the Sun during solar flares. Line detections have been made in the light of the 1.809 MeV ^{26}Al line, the 1.157 MeV ^{44}Ti line, the 847 and 1238 keV ^{56}Co lines, and the neutron capture line at 2.223 MeV.

COMPTEL has also measured the diffuse interstellar and cosmic gamma radiation, whose properties are described elsewhere (Strong et al. 1996; Strong et al. 1999; Bloemen et al. 1999a; Kappadath et al. 1996; Weidens-pointner et al. 1999). For the identification of galactic sources a modelling of the diffuse galactic emission is essential. Such a modelling at this time does not yet exist at the required degree of accuracy.

This paper is restricted to all those sources that have been definitely or marginally detected so far, and provides upper limits to the MeV flux from different types of objects. A second COMPTEL source catalogue will be produced after a detailed and accurate modelling of the diffuse interstellar emission has become possible.

The Compton Observatory was launched on April 5, 1991 by the Space Shuttle Atlantis. During Phase-I of the Compton Observatory Program, a full-sky survey - the first ever in gamma-ray astronomy - was performed. Phase-I ended on November 17, 1992. Observations during the subsequent phases of the program resulted in deeper exposures and complemented the survey. This source catalogue is mainly restricted to the results from the first five

years of the mission (up to Phase IV/Cycle-5). In a few cases, more recent results have been added.

2. Instrument description and data analysis

COMPTEL was designed to operate in the energy range 0.75 to 30 MeV. It has a large field-of-view of about 1 steradian, and different sources within this field can be resolved, if they are more than about 3 to 5 degrees away from each other (energy dependent). The resulting source location accuracy is of the order of 1°. The COMPTEL energy resolution of 5% to 10% FWHM is an important feature for gamma-ray line investigations. A detailed description of COMPTEL is given by Schönfelder et al. (1993).

COMPTEL consists of two detector assemblies, an upper one of liquid scinitillator NE213, and a lower one of NaI (Tl). A gamma-ray is detected by a Compton collision in the upper detector and a subsequent interaction in the lower detector.

The arrival direction of a detected gamma ray is known to lie on a circle on the sky. The center of each circle is the direction of the scattered gamma-ray, and the radius of the circle is determined by the energy losses E1 and E2 in both interactions. The detected photons are binned in a 3-dimensional (3-D) data space, consisting of the scatter direction (defined by the two angular coordinates χ and ψ) and by the scatter angle $\bar{\varphi}$ (derived from the measured energy losses in both interactions). Each detected photon is represented by a single point in the 3-D dataspace. The signature of a point source with celestial coordinates (χ_o, ψ_o) is a cone of 90° opening angle with its axis parallel to the $\bar{\varphi}$-axis. The apex of the cone is at (χ_o, ψ_o). Imaging with COMPTEL involves recognizing the cone patterns in the 3-D dataspace. Two main techniques are applied: one is a maximum-entropy method that generates model-independent images (Strong et al. 1992) and the other one is a maximum-likelihood method that is used to determine the statistical significance, flux and position uncertainty of a source (de Boer et al. 1992).

Significances are derived in this method from the quantity $-2\ln\lambda$, where λ is the maximum likelihood ratio $L(B)/L(B+S)$; B represents the background model and S the source model (or sky intensity model). In a point-source search, $-2\ln\lambda$ formally obeys a χ^2_3 distribution; in studies of a given source, χ^2_1 applies. [This allows to translate a measured L value into a corresponding probability for it being a noise fluctuation, equivalent to a Gaussian σ description of significances. In studies of a "known" source, $\sigma = \sqrt{-2\ln\lambda}$ applies.]

We verified by simulation that the shape of the probability density distribution for our application of the likelihood analysis to the COMPTEL data is indeed Gaussian. Furthermore, we calibrated by the same simulations the number of independent "trials" we make in a search for source, taking into account the total sky area searched (see de Boer et al. 1992).

Our threshold for detection is a chance probability of 99.7%, corresponding to a 3σ Gaussian significance. The applicable statistics, i.e. the relevant trails, are discussed for each source in the original publication.

The sensitivity of COMPTEL is significantly determined by the instrumental background. A substantial suppression is achieved by the combination of effective charged-particle shield detectors, time-of-flight measurement techniques, pulse-shape discrimination, Earth-horizon angle cuts and proper event selections in energy and $\bar{\varphi}$-space.

The application of the imaging techniques requires an accurate knowledge of the instrumental and cosmic COMPTEL background. A variety of background models has been investigated and is being used. In one method, the background is derived from averaging high-latitude observations. This assumes that the background has a constant shape in the instrumental system in at least the spatial coordinates (but not in Compton scatter angle) for all observations, and it also assumes that the extragalactic source contribution is small and smeared out by the averaging process (see Strong et al. 1999). A second method derives the background from the data that are being studied itself. This is accomplished by applying a low-pass filter to the 3-D data, which smooths the photon distribution and eliminates (in the first approximation) the source signatures (e.g. Bloemen et al. 1994). By applying iterations of this process the background estimate can be improved, further. All viewing periods have to be handled separately to account for changes of the background during the mission (Bloemen et al. 1999a). For line studies, we estimate the background below an underlying cosmic gamma-ray line by averaging the count rate from neighbouring energy intervals (Diehl et al. 1994).

For sources within the Galactic plane the global diffuse emission from the Galaxy is modelled by fitting a bremsstrahlung, and an inverse Compton component to the data. Also an isotropic component is added to these fits to represent the cosmic gamma-ray background. The amplitude of each of these components is obtained as free parameter from the fits. It has to be admitted, however (see above), that the modelling of the plane, at present, does not yet achieve the required degree of accuracy.

In addition to the normal double-scatter mode of operation, two of the NaI crystals in the lower detector assembly of COMPTEL are also operated simultaneously as burst detectors. These two modules are used to measure the time history and energy spectra of cosmic gamma-ray bursts and solar flares.

Hence, solar flares and cosmic gamma-ray bursts can be measured in the telescope mode (provided the event was within the field-of-view of the instrument), and in the burst mode.

In its telescope mode COMPTEL has an unprecedented sensitivity. Within a 2-week observation period it can detect sources, which are about 10-times weaker than

the Crab. By adding up all data from a certain source that were obtained over the entire duration of the mission, higher sensitivities can be obtained. Table 1 summarizes the achieved point-source sensitivities for a 2-week exposure in Phase-I of the mission ($t_{\rm eff} \sim 3.5\ 10^5$ s), and for the ideal cases, when all data from a certain source in the Galactic center or anticenter (where the exposure is highest) are added from either Phase-I to III ($t_{\rm eff} \sim 2.5\ 10^6$ s) or Phase-I to IV/Cycle-5 ($t_{\rm eff} \sim 6\ 10^6$ s).

From this table rough upper limits can be derived for those objects, which are not contained in the later tables 10 to 12 by deriving the effective exposure from Fig. 1.

3. The first COMPTEL source catalogue

This section consists of four different parts. The first part (Sect. 3.1) lists all observations on which the catalogue is based. Section 3.2 contains COMPTEL all-sky maps in continuum and line emission. Section 3.3 is the catalogue of detected sources, which is subdivided into detections of spin-down pulsars, galactic sources ($|b| < 10°$), active galactic nuclei, unidentified high-latitude sources, gamma-ray line sources, gamma-ray burst sources within the COMPTEL field-of-view, and solar flare detections. Section 3.4 lists COMPTEL upper limits on source candidates, namely galactic objects, active galactic nuclei, and possible gamma-ray line sources.

3.1. Observations and exposure maps

This first COMPTEL source catalogue contains mainly results from Phase-I to IV/Cycle-5 of the Compton mission. The relationship of the viewing periods (VP) to the actual dates of the observations is given in Table 2 (for completeness, the data of Phase-IV/Cycle-6 and 7 have been added in the table). The table also lists the pointing direction of the z-axis (COMPTEL telescope axis) in celestial coordinates, the duration of the pointing and the effective COMPTEL observation time.

The effective COMPTEL exposure of the entire sky from the sum of all observations from the beginning of the mission to Phase-IV/Cycle-5 and Phase IV/Cycle-7 are illustrated in Fig. 1. The deepest exposures were obtained in the Galactic center and anticenter region, where effective observation times up to $6\ 10^6$ s have been obtained (see also Table 1).

3.2. COMPTEL all-sky maps

COMPTEL all-sky maps exist for continuum emission in the three standard energy ranges $1-3$ MeV, $3-10$ MeV, and $10-30$ MeV, and for the 1.8 MeV line from radioactive ^{26}Al. These maps are shown in Figs. 2 and 3.

Figure 2 is a maximum-entropy map using all data from Phase I to Phase IV/Cycle-6 (Strong et al. 1999). The background method used in this map is based on averaging high-latitude observations (see Sect. 2).

Well known sources appear in the map:

Crab ($l = 184.5°$, $b = 5.9°$), Vela (263.6°, −2.5°) above 3 MeV, Cyg X−1 (71.1°, +3.3°), as well as striking excesses at (18°, 0°) and near the Galactic center. At higher latitudes the sky is dominated by extragalactic sources: Cen A (309°, +19°) below 10 MeV (Steinle et al. 1995), 3C 273 (290°, +64°) and 3C 279 (305°, +57°) (Williams et al. 1995b). Various "MeV blazars": 3C 454 (86°, −38°), PKS 0208−512 (276°, −62°), GRO J 0516−609 (270°, −35°) appear in one or more of the energy ranges. Next to the Crab the quasar PKS 0528+134 is clearly visible (Collmar et al. 1994; Collmar et al. 1997a). Details on these sources can be found in Blom et al. (1996) and references therein.

Note that since these sources are variable, their appearance in these time-averaged maps may not reflect their published fluxes or spectra precisely. Another interesting feature is the apparent presence of significant areas of diffuse emission away from the plane; in particular, the regions around (170°, +50°) and (85°, 35°), which have been presented as candidates for assocations with high-velocity cloud complexes (Blom et al. 1997b). Details in the structure of this emission should, however, be viewed with caution and are under further study.

An alternative approach to derive all-sky continuum maps is described in Bloemen et al. (1999a). This is a new approach combining model fitting, iterative background modelling and maximum entropy imaging, using the first five years of COMPTEL observations. On a coarse scale the maps derived by both methods are similar. However, on a fine scale, there are differences which are not yet fully understood. The uncertainties especially effect the identification of sources in the Galactic plane (see above).

Figure 3 is a COMPTEL maximum-entropy map at 1.809 MeV from all observations up to VP 522.5 (Oberlack 1997). The brightest regions are in the inner Galaxy ($-35° < l < +35°$), near Carina ($l \sim 285°$), and Vela ($l \sim 267°$). Other regions of enhanced emission are Cygnus ($l \sim 80°$), and Aquila ($l \sim 45°$).

More recently, new 1.809 MeV COMPTEL all-sky maps have been produced using different imaging and background modelling methods. In one case (Knödlseder et al. 1999) the analysis uses a multi-resolution version of the Richardson-Lucy algorithm, based on wavelets. In the other case (Bloemen et al. 1999b), the maximum entropy method is combined with model fitting and iterative background modelling. All three maps are consistent with each other within their statistical and systematic uncertainties, although the multi-resolution map shows substantially less structure along the Galactic plane.

So far, no all-sky map in the light of the 1.157 MeV ^{44}Ti gamma-ray line exists. But imaging analysis along the Galactic plane have been performed by Dupraz et al.

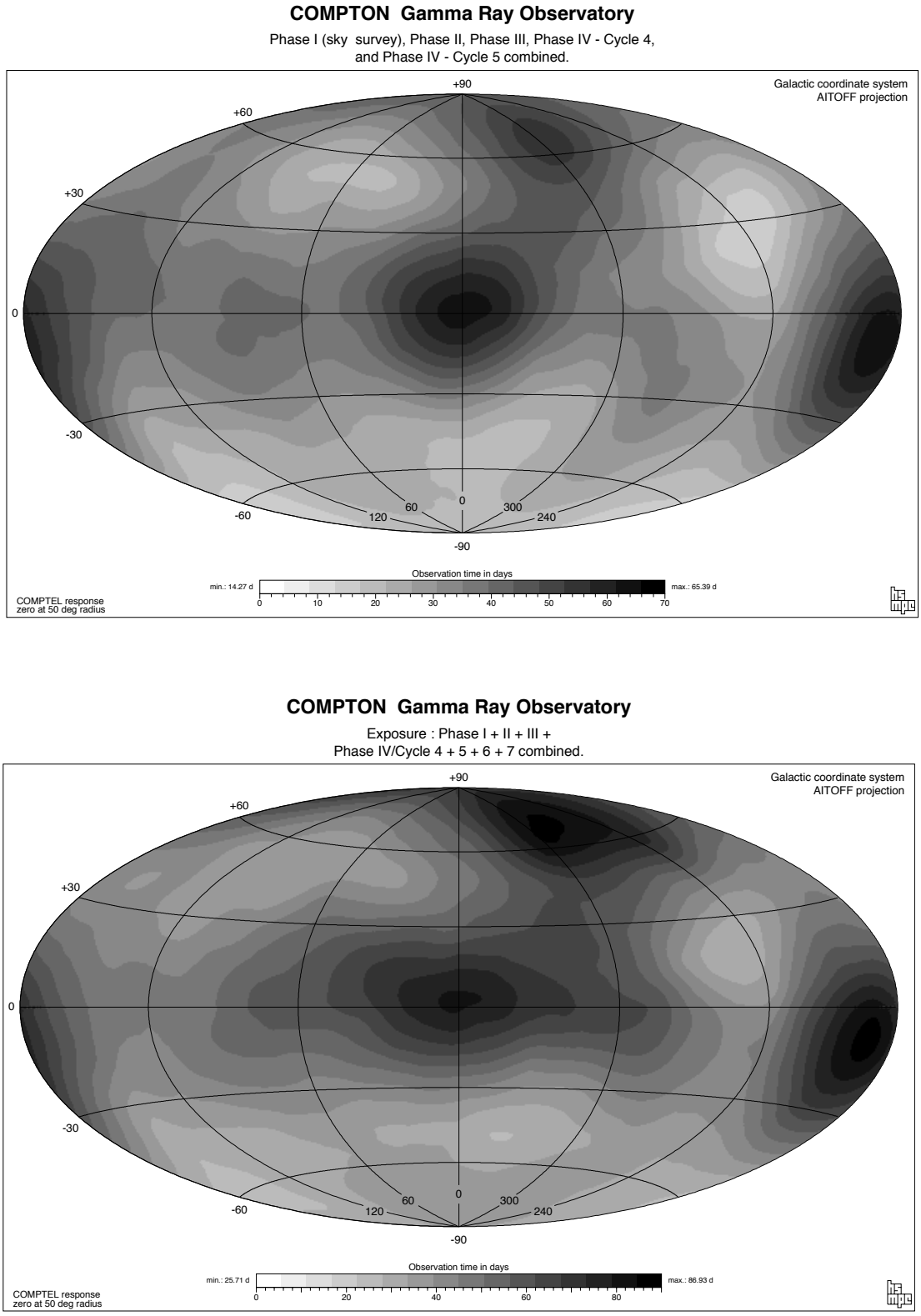

Fig. 1. Effective exposure of COMPTEL from the sum of all observations. Top: Sum of all observations up to Phase IV/Cycle-5. Bottom: Sum of all observations up to Phase IV/Cycle-7

Table 1. COMPTEL 3σ point source sensitivity limits

	3σ Flux Limits [10^{-5} photons cm^{-2} s^{-1}]		
E_γ[MeV]	2 weeks in Phase 1	Phase 1+2+3	Phase 1+2+3+4 (Cycle-5)
$0.75-1$	20.1	7.4	3.7
$1-3$	16.8	5.5	3.8
$3-10$	7.3	2.8	1.7
$10-30$	2.8	1.0	0.8
1.157	6.2	2.0	1.6
1.809	6.6	2.2	1.6

Note. From this table rough upper limits can be derived for those objects, which are not contained in the later Tables 10 to 12 by deriving the effective exposure from Fig. 1.

(1997) for data from Phases I to III, and by Iyudin et al. (1999) from Phases I to IV/Cycle-6. Two ^{44}Ti gamma-ray line sources have been discovered so far, these are Cas A (Iyudin et al. 1997a) and GRO J 0852 − 4642 (Iyudin et al. 1998), a supernova remnant near the Vela region (Aschenbach 1998).

A maximum-entropy map in the light of the 2.2 MeV neutron-capture line based on data from the first five years of the mission (VP 1.0 through VP 523.0) has been produced by Mcconnell et al. (1997b). In general, the sky at 2.2. MeV is relatively featureless, e.g. the galactic plane is not visible. There is, however, evidence for significant ($\sim 3.7\sigma$) emission from a point-like feature near $(l, b) = (300.5°, -29.6°)$, the origin of which remains unknown at this time (McConnell et al. 1997b). Flux limits for any candidate source are typically in the range (1 to 2.0) 10^{-5} cm^{-2} s^{-1} (at the 3σ significance level).

Figure 4 is an all-sky map of the statistical location contours of 31 gamma-ray bursters, which happened to be in the COMPTEL field-of-view from the beginning of the mission up to viewing period 419.5 (Kippen et al. 1998a).

3.3. COMPTEL source detections

The COMPTEL source detections are summarized in Tables 3 to 9:

- Table 3: Detected Spin-Down Pulsars.
- Table 4: Galactic Sources $|b| < 10°$.
- Table 5: Active Galactic Nuclei.
- Table 6: Unidentified High-Latitude Sources.
- Table 7: Gamma-Ray Line Sources.
- Table 8: Gamma-Ray Burst Locations.
- Table 9: Solar-Flare Detections.

Out of the 7 spin-down pulsars listed in Table 4 COMPTEL has made firm detections from PSR B0531+21 (Crab), PSR B0833−45 (Vela), and from PSR B1509−58. The analysis of the Vela pulsar, however, is not yet finally settled; the results presented are presently based on Phases 0 and I, only. Because of the good statistics, the Crab pulsar fluxes are listed for smaller energy intervals than the standard ones ($0.75-1$, $1-3$, $3-10$ and $10-30$ MeV). Only indications for emission in the COMPTEL energy range were found from the four pulsars PSR B1951+32, PSR J0633+1746 (Geminga), PSR 0656+14, and PSR B1055−52.

The Galactic Sources with $|b| < 10°$ listed in Table 4 are all objects, which were seen by at least one other experiment of the Compton Observatory. These are Cyg X−1, the two EGRET sources 2EG 2227+61 and 2EG J0241+6119 (which both are also COS-B sources), Nova Persei 1992 (GRO J0422+32), the Crab nebula, and an unidentified bright source at $l = 18°$ within the plane (coincident with the EGRET source 2ES J1825−1307). The COMPTEL fluxes for these sources are listed in the standard energy ranges. For some of the sources the fluxes are also given for other energy intervals. The possible contribution of the diffuse galactic emission to the listed source fluxes constitutes a basic uncertainty (see Col. 11 of the table).

Nine of the Active Galactic Nuclei listed in Table 5 are of the γ-ray Blazar type, discovered by EGRET (with the exception of 3C 273, earlier discovered by COS-B, Swanenburg et al. (1978). The only non-blazar type object in the table is the radio galaxy Cen A. All γ-ray blazars are highly variable in intensity.

Three of the five unidentified high-latitude sources in Table 6 are not point-like, but cover an extended region. Their extent may actually be due to a larger number of - so far - unresolved point sources (GRO J1823−12 and the two High-Velocity Cloud complexes).

The gamma-ray line sources listed in Table 7 are ordered with increasing line-energy. Apart from the four point-like sources SN 1991T, Cas A, Carina, and the SNR GRO J0852−4642, also the three extended emission regions of the inner Galaxy and of the Cygnus and Vela regions are included in the table.

The 31 gamma-ray bursts listed in Table 8 were all recorded in the "telescope mode". The error radius of the burst location (Col. 4) is defined as the angular radius, having the same area as the irregularily shaped COMPTEL 1σ confidence region (see also Fig. 5). Columns 5, 6, and 7 provide informations on the COMPTEL accumulation time, the measured 0.75 to 30 MeV fluence and the COMPTEL detection significance of each burst. The parameters for a power-law fit

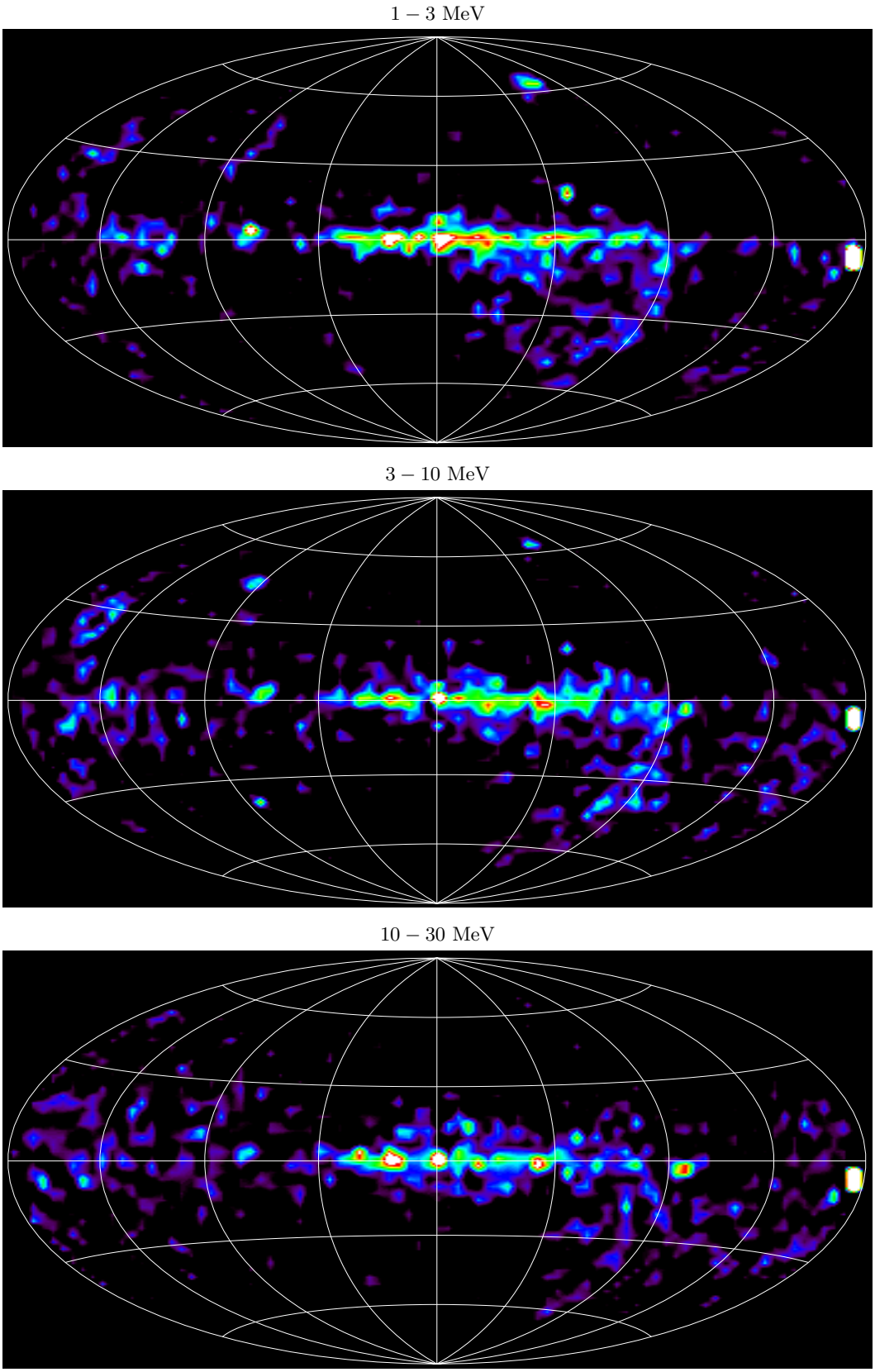

Fig. 2. Full-sky maximum entropy intensity maps from all data between Phases I to IV/Cycle-6. Energy ranges are (from top to bottom): $1-3$ MeV, $3-10$ MeV, $10-30$ MeV (from Strong et al. 1999)

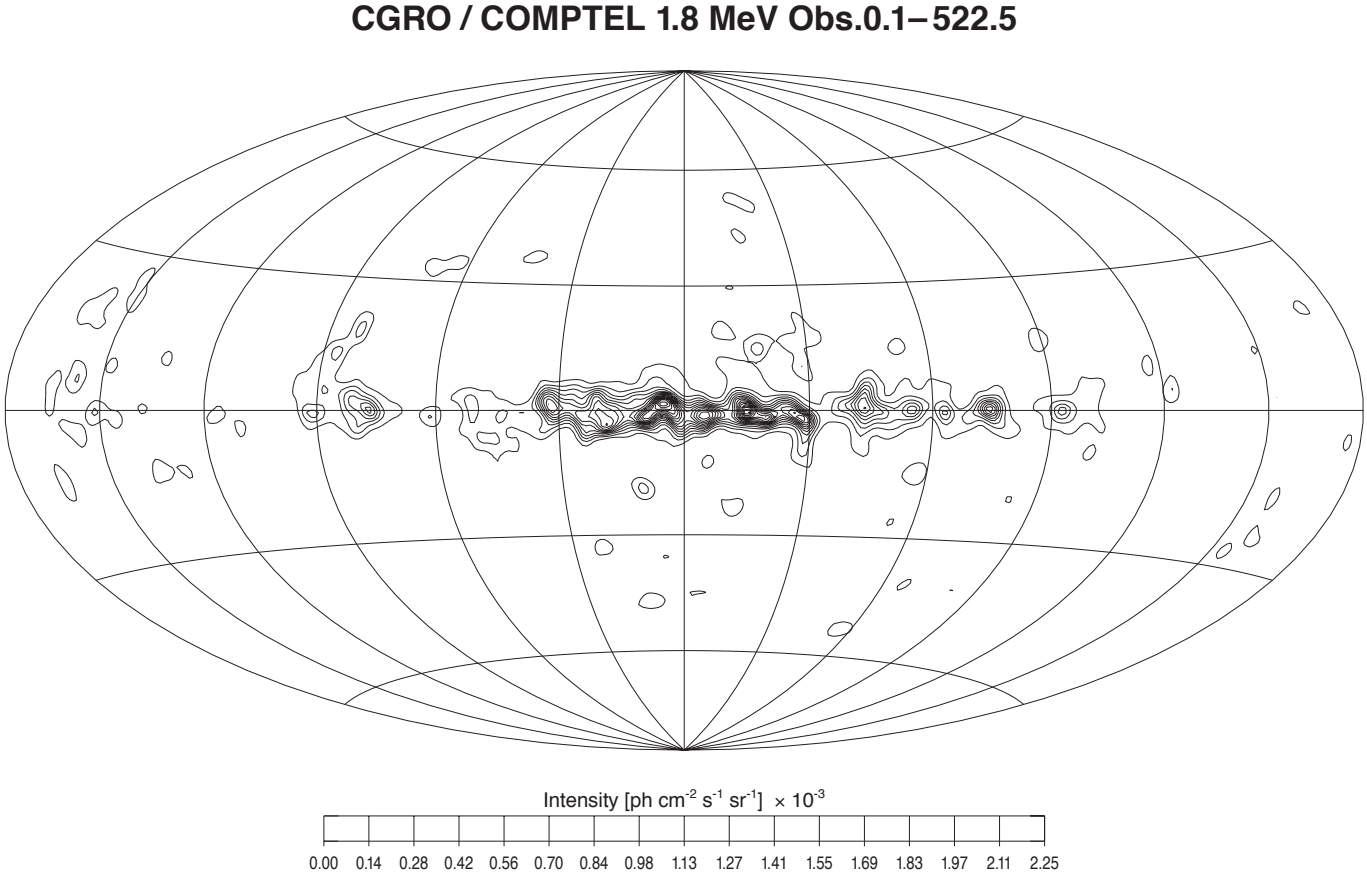

Fig. 3. COMPTEL maximum entropy map from VP 1 to VP 522.5 at 1.809 MeV (from Oberlack 1997)

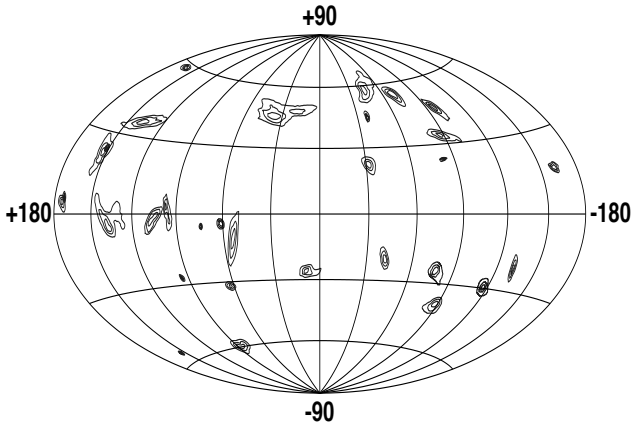

Fig. 4. Statistical (1-, 2-, and 3-sigma) location contours, in Galactic coordinates of 29 gamma-ray bursts observed through viewing period 419.5. The extent of the contours depends on the strength of the burst (from Kippen et al. 1998a)

to the spectrum of each burst are listed in Cols. 8 and 9. Column 10 states, whether variability of the burst spectrum during accumulation was observed in the more sensitive "burst mode".

Solar Flare gamma-ray measurements taken in the burst mode are summarized in Table 9. Column 1 contains the COMPTEL flare identification, including the year/month/day and UT of the flare start (taken from the GSFC Solar Data Analysis Center (SDAC)). Truncated Julian Day, in Col. 2 and Col. 3, contains the GOES X-ray start time (taken from the Solar Geophysical Reports). The X-ray classification is in Col. 4 and the BATSE flare number, as assigned at the SDAC at Goddard Space Flight Center, is in Col. 5. The corresponding BATSE trigger number is in Col. 2. The COMPTEL data measured in this burst mode (see Sect. 6) have been inspected and the flare (integration time) duration as judged by the visible signal in the spectrometer is listed in Col. 7 with the corresponding integrated counts in the full energy range in Col. 8. The peak counts (with an integration time of x s) are listed in Col. 9. The peak count rate as measured by BATSE is in Col. 10 as obtained from the SDAC at GSFC. Finally, in Col. 11 is the integrated amount of spacecraft and instrument material between the spectrometer and the Sun. This material attenuates the gamma-ray flux and degrades the spectrum. A small number is better. Large amounts of intervening material can, in principle, be

modeled away when producing a photon spectrum, but the results have large errors and are often not unique.

3.4. COMPTEL upper limits to source candidates

The limits are given at the 2σ confidence level for the following objects:

- Table 10: Galactic Objects $|b| < 10°$.
- Table 11: Active Galactic Nuclei.
- Table 12: Possible Sources of Gamma-Ray Line Emission.

Table 10 contains upper limits to Galactic Sources with $|b| < 10°$. This source list is restricted to black-hole candidates. Due to the above mentioned, still existing, uncertainty in modelling the diffuse Galactic emission, the source limits are at present rather conservative.

Presented in Tables 11a and 11b are the cumulative two-sigma upper limits to the MeV-emission measured with COMPTEL from active galactic nuclei (AGN) and other unidentified gamma-ray sources detected at high Galactic latitudes. These limits were derived using composite COMPTEL all-sky maximum-likelihood maps for the 4.5 year period covering Phases I through IV/Cycle-4 of the CGRO mission (1991-1995). A description of the data-processing procedure used to obtain the composite all-sky maps can be found in Stacy et al. (1997).

In the choice of candidate objects, emphasis was placed on known or suspected gamma-ray sources, particularly those detected in neighbouring energy bands to COMPTEL by the CGRO/EGRET and OSSE instruments (e.g., von Montigny et al. 1995; McNaron-Brown et al. 1995). The flux-extraction routine applied to the composite all-sky maps computes average output values within one-pixel radius of a specified source location. To minimize the number of spurious false detections, only those objects for which the summed log-likelihood ratio exceeds the equivalent of a three-sigma source detection (adopting χ^2_1 statistics, appropriate for a previously known source at a specified location) are considered to exhibit potentially significant MeV emission.

Table 11a lists the COMPTEL cumulative upper limits for MeV-emission from AGN through Phase IV/Cycle-4 of the CGRO mission. Column 1 gives the object name in coordinate format; Col. 11 gives another common name for the source; Col. 10 lists the object "type", which is either the object class (SY for Seyfert galaxy, from the target list of Maisack et al. 1995), or a reference to a previously reported gamma-ray detection of this source (1EG for the First EGRET Catalog of Fichtel et al. 1994, 2EG for the Second EGRET Catalog of Thompson et al. 1995, 2EGS for the Supplement to the Second EGRET Catalog of Thompson et al. 1996).

Table 11b lists the COMPTEL cumulative upper limits for MeV-emission from unidentified high-latitude gamma-ray sources detected by the CGRO/EGRET instrument. In both Tables 11a and 11b the recommended COMPTEL team-standard corrections (for time-of-flight effects, live-time, etc.) are applied to obtain final fluxes and upper limits (see Diehl 1996).

Inspection of Tables 11a and 11b shows only in a few isolated cases the cumulative detection with COMPTEL of significant emission from high-latitude sources. This is no contradiction to the detections listed in Table 5. Note that all these sources are time-variable, and their detection in individual viewing periods does not mean that they are visible in cumulative maps.

In general, the flux limits presented in Table 11a show that COMPTEL does not detect cumulative MeV-emission from a majority of the extragalactic blazar sources detected by EGRET. This result is similar to that obtained by Blom (1997), for the case of individual CGRO viewing periods. Ultimately, these cumulative results will be further compared with other source studies for individual CGRO viewing periods, and used in statistical investigations of source properties by object class (e.g. Blom 1997; Williams et al. 1997).

The upper limits to possible sources of gamma-ray line emission in Table 12 are again ordered with increasing line energies. The line sources considered are SN 1993J (^{56}Ni $\rightarrow$ ^{56}CO $\rightarrow$ ^{56}Fe decay), four supernovae as possible ^{44}Ti line emitters at 1.157 MeV, eleven recent novae as possible sources of ^{22}Na line emission at 1.275 MeV, five nebula or cloud complexes as 1.809 MeV ^{26}Al sources, and six possible 2.223 MeV neutron capture sources.

4. Conclusion

COMPTEL has opened the MeV gamma-ray band (0.75 to 30 MeV) as a new window to astronomy. The data from five years of COMPTEL observations provided the first COMPTEL source catalogue. It is largely restricted to previously published results, and contains firm as well as marginal detections of continuum and line emitting sources, and presents upper limits for various types of objects. The number of most significant detections ($> 3\sigma$) are 32 for steady sources and 31 for gamma-ray bursters (see Table 13). Six of the listed sources extend over larger areas. Their extent may actually be due to a larger number of so far unresolved point sources. This may be especially true for the Cygnus region in 1.809 MeV, for GRO J1823−12 and for the two HVC complexes. A second COMPTEL source catalogue will be produced after a more accurate modelling of the diffuse interstellar emission has become possible.

Acknowledgements. The COMPTEL project is supported by the German government through DLR grant 50 Q 9096 8, by NASA under contract NAS5-26645, and by the Netherlands Organization for Scientific Research NWO. The authors acknowledge the efforts of M. Chupp, H. Haber, J. Englhauser and R. Georgii in implementing the various tables.

References

Aschenbach B., 1998, Nat 396, 141

Bennett K., Schönfelder V., Ryan J., et al., 1993, IAU Circ. 5749

Bloemen H., Hermsen W., Swanenburg B.N., et al., 1994, ApJS 92, 419

Bloemen H., Bennett K., Blom J.J., et al., 1995, A&A 293, L1

Bloemen H., Hermsen W., Kappadath S.C., et al., 1999a, Proc. of 3rd INTEGRAL Workshop, Taormina, Italy, September 14-18, 1998, Palumbo G., Bazzano A., Winkler C. (eds.), Astrophys. Lett. Comm. 39, 213/[681]-216[684]

Bloemen H., Diehl R., Hermsen W., et al., 1999b, Proc. of 3rd INTEGRAL Workshop, Taormina, Italy, September 14-18, 1998, Palumbo G., Bazzano A., Winkler C. (eds.), Astrophys. Lett. Comm. 38, 391-398

Blom J.J., 1997, Ph.D. Thesis, University of Leiden, The Netherlands

Blom J.J., Bloemen H., Bennett K., et al., 1995a, A&A 295, 330

Blom J.J., Bennett K., Bloemen H., et al., 1995b, A&A 298, L33

Blom J.J., Bennett, K., Bloemen H., et al., 1996, A&AS 120, 507

Blom J.J., Bloemen H., Bykov A.M., et al., 1997a, Proc. of 2nd INTEGRAL Workshop, Winkler C., Courvoisier T.J.-L., Durouchoux Ph. (eds.), ESA SP-382, p. 119

Blom J.J., Bloemen H., Bykov A.M., et al., 1997b, A&A 321, 288

Collmar W., Bennett K., Bloemen H., et al., 1993, A&AS 97, 71

Collmar W., Bennett K., Bloemen H., et al., 1994, Proc. 2nd Compton Symposium, AIP Conf. Proc. 304, Fichtel C.E., Gehrels N., Norris J.P. (eds.), p. 659

Collmar W., Bennett K., Bloemen H., et al., 1996, A&AS 120, 515

Collmar W., Bennett K., Bloemen H., et al., 1997a, A&A 328, 33

Collmar W., Wessolowski U., Schönfelder V., et al., 1997b, Proc. of 4th Compton Symposium, 1997, Dermer C.D., Strickman M.S., Kurfess J.D. (eds.). AIP New York 410, p. 1587

Collmar W., Blom J.J., Bennett K., et al., 1997c, Proc. of 25th ICRC, Durban, Potgieter M.S., Raubenheimer B.C., der Walt D.J. v. (eds.), Vol. 3, p. 101

Connors A., Aarts H.J.M., Bennett K., et al., 1993a, A&AS 97, 75

Connors A., Collmar W., Hanlon L., 1993b, Adv. Space Res. 13(12), 715

Connors A., Bennett K., Collmar W., et al., 1997, Proc. of 25th ICRC, Durban, Potgieter M.S., Raubenheimer B.C., der Walt D.J. v. (eds.), Vol. 3, p. 13

de Boer H. Bennett K., Bloemen H., et al., 1992 in: Data Analysis in Astron. IV, di Gesù V., Scarsi L., Buccheri R., Crane P., Maccarone M.C., Zimmermann H.U. (eds.). Plenum Press, New York, p. 241

del Rio E., v. Ballmoos P., Bennett K., et al., 1996, A&A 315, 237

Diehl R., 1996, "COMPTEL Data Analysis Standards", COMPTEL Internal Report COM-MO- DRG-MGM-231.9 (3 March 1996)

Diehl R., Dupraz C., Bennett K., et al., 1994, ApJS 92, 429

Dupraz C., Bloemen H., Bennett K., et al., 1997, A&A 324, 683

Fichtel C.E., Bertsch D.E., Chiang J., et al., 1994, ApJS 94, 551 (1EG)

Greiner J., Sommer M., Bade N., et al., 1995, A&A 302, 121

Hanlon L.O., Bennett K., Williams O.R., et al., 1994a, A&A 285, 161

Hanlon L.O., Bennett K., Williams O.R., et al., 1994b, in: AIP Conf. Proc. No. 307; Gamma-Ray Bursts, Fishman G.J., Brainerd J.J., Hurley K. (eds.). New York: AIP Press, p. 275

Hanlon L.O., Hermsen W., Kippen R.M., et al., 1995, A&A 296, L41

Hermsen W., Kuiper L., Schönfelder V., et al., 1997, Proc. of 2nd INTEGRAL Workshop, Winkler C., Courvoisier T.J.-L., Durouchoux Ph. (eds.), ESA-SP 382, 287

Iyudin A.F., Diehl R., Bloemen H., et al., 1994, A&A 284, L1

Iyudin A.F., Bennett K., Bloemen H., et al., 1995, A&A 300, 422

Iyudin A.F., Bennett K., Bloemen H., et al., 1996, A&A 311, L21

Iyudin A., Diehl R., Lichti G.G., et al., 1997a, Proc. of 2nd INTEGRAL Workshop, Winkler C., Courvoisier T.J.-L., Durouchoux Ph. (eds.), ESA-SP 382, p. 37

Iyudin A., Reimer O., Bennett K., et al., 1997b, Proc. of 25th ICRC, Durban, Potgieter M.S., Raubenheimer B.C., der Walt D.J. v. (eds.), Vol. 3, p. 89

Iyudin A., Schönfelder V., Bennett K., et al., 1998, Nat 396, 142

Iyudin A., Schönfelder V., Bennett K., et al., 1999, Proc. of 3rd INTEGRAL Workshop, Taormina, Italy, September 14-18, 1998, Palumbo G., Bazzano A., Winkler C. (eds.), Astrophys. Lett. Comm. 38, 383-386

Kappadath S.C., Ryan J., Bennett K., 1996, A&AS 120, 619

Kippen R.M., 1995d, Ph.D. Thesis, University of New Hampshire, Durham N.H., U.S.A.

Kippen R.M., Connors A., Collmar W., et al., 1993, Proc. of 23rd ICRC, The University of Calgary 1, 85

Kippen R.M., Macri J., Ryan J., et al., 1994a, IAU Circ. 5937

Kippen R.M., Macri J., Ryan J., et al., 1994b, IAU Circ. 5943

Kippen R.M., Connors A., Macri J., et al., 1994c, in: AIP Conf. Proc. 307, Gamma-Ray Bursts, Fishman G.J., Brainerd J.J., Hurley K. (eds.). New York: AIP Press, p. 420

Kippen R.M., Connors A., McConnell M., et al., 1995a, Adv. Space Res. 15(5), 139

Kippen R.M., Bennett K., Connors A., et al., 1995b, A&A 293, L5

Kippen R.M., Ryan J., Connors A., et al., 1995c, Ann. N.Y. Acad. Sci. 759, 425

Kippen M., Ryan J., Connors A., et al., 1996, in AIP Conf. Proc. 384, Gamma-Ray Bursts, Kouveliotou C., Briggs M.S., Fishman G.J. (eds.). New York AIP, p. 436

Kippen M., Ryan J., Connors A., et al., 1998a, Adv. Sp. Res. 22(7), 1097

Kippen M., Ryan J., Connors A., et al., 1998b, ApJ 492, 246

Knödlseder J., Chen W., Oberlack U., Diehl R., Gehrels N., 1996, A&AS 120, 339

Knödlseder J., Bennett K., Bloemen H., et al., 1999, A&A 345, 813

Kuiper L., Hermsen W., Bennett K., et al., 1996, A&AS 120, 73

Kuiper L., Hermsen W., Bennett K., et al., 1998a, A&A 337, 421
Kuiper L., Hermsen W., Schönfelder V., et al., 1998b, NATO ASI Ser. C 515, 211
Kuiper L., Hermsen W., Krijger J., et al., 1999a, Proc. of 3rd INTEGRAL Workshop, Taormina, Italy, September 14-18, 1998, Palumbo G., Bazzano A., Winkler C. (eds.), Astrophys. Lett. Comm. 38, 33-36
Kuiper L., Hermsen W., Krijger J., et al., 1999b, A&A 351, 119
Lichti G.G., Iyudin A., Bennett K., et al., 1996, A&AS 120, 353
Maisack M., Collmar W., Barr P., et al., 1995, A&A 298, 400
McConnell M., Forrest D., Ryan J., et al., 1994, ApJ 424, 933
McConnell M., Bennett K., Bloemen H., et al., 1996, A&AS 120, 149
McConnell M., Bennett K., Bloemen H., et al., 1997a, Proc. of 25th ICRC, Durban, South Africa, Potgieter M.S., Raubenheimer B.C., der Walt D.J. v. (eds.), Vol. 3, p. 93
McConnell M., Bennett K., Bloemen H., et al., Proc. of 4th Compton Symposium, 1997b, Dermer C.D., Strickman M.S., Kurfess J.D. (eds.). AIP New York 410, p. 1099
McNaron-Brown K., Johnson W.N., Jung G.V., et al., 1995, ApJ 451, 575
Morris D., Bennett K., Bloemen H., et al., 1995, Ann. N.Y. Acad. Sci. 759, 397
Much R., Bennett K., Buccheri R., et al., 1995a, A&A 299, 435
Much R., Bennett K., Buccheri R., et al., 1995b, Adv. Sp. Res. 15(5), 81
Much R., Bennett K., Winkler C., 1997, Proc. of 4th Compton Symposium, 1997, Dermer C.D., Strickman M.S., Kurfess J.D. (eds.). AIP New York 410, p. 542
Oberlack U., 1997, Ph.D. Thesis, Technical University Munich, Germany
Oberlack U., Bennett K., Bloemen H., et al., 1995, Proc. of 24th ICRC, Istituto Nazionale Fisica Nucleare, Rome, Vol. 2, p. 207
Ryan J., Kippen M., Varendorff M., 1993, IAU Circ. 5702
Ryan J.M., McConnell M., Kippen R.M., et al., 1994a, IAU Circ. 5950
Ryan J.M., Bennett K., Collmar W., et al., 1994b, ApJ 422, L67
Schaefer B.E., Teegarden B.J., Cline T.L., et al., 1994, in: AIP Conf. Proc. No. 307, Gamma-Ray Bursts, Fishman G.J., Brainerd J.J., Hurley K. (eds.). New York: AIP Press, p. 280
Schönfelder V., 1991, IAU Circ. 5369
Schönfelder V., Aarts H., Bennett K., 1993, ApJS 86, 657
Schönfelder V., Bennett K., Bloemen H., et al., 1995, Ann. N.Y. Acad. Sci. 759, 226
Schönfelder V., Bennett K., Bloemen H., et al., 1996, A&AS 120, 13
Share G.H., Connors A., Dingus B.L., et al., 1994, in: AIP Conf. Proc. No. 307, Gamma-Ray Bursts, Fishman G.J., Brainerd J.J., Hurley K. (eds.). New York: AIP Press, p. 283
Stacy J.G., Ryan J.M., Collmar W., et al., 1997, Proc. of 4th Compton Symposium, Dermer C.D., Strickman M.S., Kurfess J.D. (eds.). AIP New York 410, p. 1356
Steinle H., Collmar W., Diehl R., et al., 1995, Adv. Space Res. 15, 37
Steinle H., Bennett K., Bloemen H., et al., 1998, A&A 330, 97
Strong A.W., Cabeza-Orcel P., Bennett K., et al., 1992, in: Data Analysis in Astron. IV, di Gesù V., Scarsi L., Buccheri R. et al. (eds.). Plenum Press, New York, p. 251-260
Strong A.W., Bennett K., Bloemen H., 1996, A&AS 120, 381-388
Strong A.W., Bloemen H., Diehl R., et al., 1999, Proc. of 3rd INTEGRAL Workshop, Taormina, Italy, September 14-18, 1998, Palumbo G., Bazzano A., Winkler C. (eds.), Astrophys. Lett. Comm. 39, 209/[667]-212[680]
Swanenburg B.N., Bennett K., Bignami G.F., et al., 1978, Nat 275, 298
Thompson D.J., Bertsch D.L., Dingus B.L., et al., 1995, ApJS 101, 259 (2EG)
Thompson D.J., Bertsch D.L., Dingus B.L., et al., 1996, ApJS 107, 227 (2EGS)
Thompson D.J., Bailes M., Bertsch D.L., et al., 1999, ApJ 516, 297
van der Meulen R.D., Bloemen H., Bennett K., et al., 1998, A&A 330, 321
van der Meulen R.D., Bloemen H., Bykov A.M., et al., 1999, Proc. of 3rd INTEGRAL Workshop, Taormina, Italy, September 14-18, 1998, Palumbo G., Bazzano A., Winkler C. (eds.), Astrophys. Lett. Comm. 38, 367-370
van Dijk R., Bennett K., Collmar W., et al., 1995, A&A 296, L33
van Dijk R., 1996, Ph.D. Thesis, University of Amsterdam, The Netherlands
Varendorff M.G., Bennett K., de Boer H., et al., 1992, in: AIP Conf. Proc. No. 265, Gamma-Ray Bursts, Paciesas W.S., Fishman G.J. (eds.). New York: AIP Press, p. 22
Varendorff M.G., Connors A., Collmar W., et al., 1993, Proc. of 23rd ICRC, University of Calgary 1, 81
von Montigny C., Bertsch D.L., Chiang J., et al., 1995, ApJ 440, 525
Weidenspointner G., Varendorff M., Bennett K., et al., 1999, Proc. of 3rd INTEGRAL Workshop, Taormina, Italy, September 14-18, 1998, Palumbo G., Bazzano A., Winkler C. (eds.), Astrophys. Lett. Comm. 39, 193/[661]-196[664]
Williams O.R., Much R., Bennett K., et al., 1995, A&A 297, L21
Williams O.R., Bennett K., Bloemen H., et al., 1995b, A&A 298, 33
Williams O.R., Bennett K., Much R., et al., 1997, Proc. of 4th Compton Symposium, 1997, Dermer C.D., Strickman M.S., Kurfess J.D. (eds.). AIP New York 410, p. 1582
Williams O.R., Bennett K., Much R., et al., 1999, Proc. of 5th Compton Symposium (Portsmouth N.H., U.S.A.). AIP N.Y. (submitted for publication)
Winkler C., Bennett K., Bloemen H., et al., 1992, in: AIP Conf. Proc. No. 265, Gamma-Ray Bursts, Paciesas W.S., Fishman G.J. (eds.). New York: AIP Press, p. 77
Winkler C., Bennett K., Bloemen H., et al., 1993a, A&A 255, L9
Winkler C., Bennett K., Hanlon L., et al., 1993b, in: AIP Conf. Proc. No. 280, Gamma-Ray Observatory, Friedlander M., Gehrels N., Macomb D.J. (eds.). New York: AIP Press, p. 845
Winkler C., Kippen R.M., Bennett K., et al., 1995, A&A 302, 765

Table 2. COMPTEL observations, pointings and viewing periods

Phase I

Viewing Period	start (yy-mm-dd)	Z-axis pointing	galactic LONG	galactic LAT	duration (days)	eff. COMPTEL observing time (days)
1.0	91-05-16	Crab pulsar	190.9	−4.7	14	5.3
2.0	91-05-30	Cyg X−1	73.3	2.6	9	3.8
2.5	91-06-08	Sun	194.9	−7.3	7	3.5
3.0	91-06-15	SN 1991T	299.8	65.5	13	5.5
4.0	91-06-28	NGC 4151	156.2	72.1	14	4.8
5.0	91-07-12	Gal. Center	0.0	−4.0	14	5.0
6.0	91-07-26	SN 1987A	278.0	−29.3	13	3.9
7.0	91-08-08	Cyg X−3	70.4	−8.3	7	3.5
7.5	91-08-15	gal. 025−14	25.0	−14.0	7	2.3
8.0	91-08-22	Vela Pulsar	262.9	−5.7	14	4.6
9.0	91-09-05	gal. 339−84	338.9	−83.5	7	2.5
9.5	91-09-12	Her X−1	59.7	40.3	7	2.9
10.0	91-09-19	Fairall 9	287.9	−54.3	14	4.4
11.0	91-10-03	3C 273	294.3	63.7	14	5.3
12.0	91-10-17	Centaurus A	310.7	22.2	14	4.5
13.0	91-10-31	gal. 025−14	25.0	−14.0	7	2.8
13.5	91-11-07	gal. 339−84	338.9	−83.5	7	2.5
14.0	91-11-14	Eta Carinae	285.0	−0.7	14	3.2
15.0	91-11-28	NGC 1275	152.6	−13.4	14	5.9
16.0	91-11-12	Sco X−1	0.0	20.3	15	5.6
17.0	91-12-27	SN 1987A	283.2	−31.6	14	4.1
18.0	92-01-10	M 82	137.5	40.5	13	5.1
19.0	92-01-23	gal. 058−43	58.2	−43.0	14	5.5
20.0	92-02-06	SS 433	39.7	0.8	14	5.8
21.0	92-02-20	NGC 1068	171.5	−53.9	14	4.5
22.0	92-03-05	MRK 279	112.5	44.5	14	4.5
23.0	92-03-19	Cir X−1	322.1	3.0	14	2.2
24.0	92-04-02	gal. 010 57	9.5	57.2	7	1.7
24.5	92-04-09	gal. 010 57	9.5	57.2	7	1.8
25.0	92-04-16	gal. 007 48	6.8	48.1	7	1.8
26.0	92-04-23	MRK 335	108.8	−41.4	5	1.0
27.0	92-04-28	4U 1543−47	332.2	2.5	9	1.7
28.0	92-05-07	MRK 335	108.8	−41.4	7	1.8
29.0	92-05-14	gal. 224−40	224.0	−40.0	21	4.4
30.0	92-06-04	NGC 2992	252.4	30.7	7	1.7
31.0	92-06-11	MCG 8−11−11	163.1	11.9	14	5.2
32.0	92-06-25	NGC 3783	284.2	22.9	7	1.4
33.0	92-07-02	NGC 2992	252.4	30.7	14	2.8
34.0	92-07-16	Cas A	108.8	−2.4	21	3.6
35.0	92-08-06	ESO 141−55	335.1	−25.6	5	0.9
36.0	92-08-11	GRO J0422 32	169.8	−11.4	1	0.3
36.5	92-08-12	GRO J0422 32	168.2	−9.5	8	2.0
37.0	92-08-20	MRK 335	104.8	−42.1	7	1.8
38.0	92-08-27	ESO 141−55	335.1	−25.6	5	1.0
39.0	92-09-01	GRO J0422 32	167.2	−9.2	16	4.0
40.0	92-09-17	MCG 5−23−16	195.9	44.7	21	5.6
41.0	92-10-08	gal. 228 03	228.0	2.8	7	1.5
42.0	92-10-15	PKS 2155−304	0.0	−44.6	14	2.4
43.0	92-10-29	MRK 509	31.1	−28.3	5	1.2
44.0	92-11-03	gal. 228 03	228.0	2.8	14	3.2
	92-11-17	end of Phase I				
201.0	92-11-17	Her X−1	66.8	39.3	7	1.1
202.0	92-11-24	Her X−1	70.9	40.5	7	1.2
203.0	92-12-01	Cygnus	77.9	0.7	7	2.0
203.3	92-12-08	Cygnus	77.9	0.7	7	2.0
203.6	92-12-15	Cygnus	77.9	0.7	7	2.0
204.0	92-12-22	3C 273	294.7	61.9	7	2.0
205.0	92-12-29	3C 273	294.5	61.6	7	2.0
206.0	93-01-05	3C 273	294.7	61.9	7	1.9
207.0	93-01-12	IC 4329A	314.1	31.5	21	4.8
208.0	93-02-02	NGC 4507	307.4	20.8	7	1.5
209.0	93-02-09	2CG 010−31	0.2	−34.0	13	3.9
210.0	93-02-22	Gal. Center	355.6	6.3	3	0.6
211.0	93-02-25	gal. 123−05	125.9	−4.7	12	3.2
212.0	93-03-09	WR 140	83.7	11.7	14	3.9
213.0	93-03-23	Crab Pulsar	182.6	−8.2	6	1.1

Table 2. continued

Phase II

Viewing Period	start (yy-mm-dd)	Z-axis pointing	galactic LONG	galactic LAT	duration (days)	eff. COMPTEL observing time (days)
214.0	93-03-29	Gal. Center	355.6	6.3	3	0.7
215.0	93-04-01	Centaurus A	311.7	22.9	5	1.1
216.0	93-04-06	SN 1993J	140.8	38.1	6	1.3
217.0	93-04-12	Centaurus A	311.7	22.9	8	1.8
218.0	93-04-20	NGC 4151	151.4	71.3	14	2.7
219.1	93-05-04	reboost testing				
219.4	93-05-05	Gal. Center	350.1	15.9	2	0.5
219.7	93-05-07	reboost calibration burn				
220.0	93-05-08	SMC	298.1	−44.6	5	0.9
221.0	93-05-13	Crab Pulsar	187.5	−5.9	11	2.3
222.0	93-05-24	NGC 4151	157.8	70.6	7	2.0
223.0	93-05-31	Gal. Center	359.1	−0.1	3	0.7
224.0	93-06-03	SMC	298.1	−44.6	12	1.8
225.0	93-06-15	reboost				
226.0	93-06-19	gal. 355 05	355.0	5.0	9	2.1
227.0	93-06-28	SN 1993J	148.1	41.2	15	3.3
228.0	93-07-13	SN 1993J	149.9	42.7	14	3.1
230.0	93-07-27	Vela region	276.7	−2.3	3	0.7
230.5	93-07-30	Vela region	278.8	1.4	4	0.9
231.0	93-08-03	NGC 6814	22.2	−13.1	7	1.5
229.0	93-08-10	gal. 5 05	5.0	5.0	1	0.2
229.3	93-08-11	Perseid meteor shower				
229.5	93-08-12	gal. 5 05	5.0	5.0	5	1.1
301.0	93-08-17	Vela Pulsar	263.6	−2.7	7	1.2
232.0	93-08-24	gal. 348 00	347.5	0.0	2	0.4
232.5	93-08-26	gal. 348 00	347.5	0.0	12	2.6
	93-09-07	end of Phase II				
301.0	93-08-17	Vela Pulsar	263.6	−2.7	7	1.2
232.0	93-08-24	gal. 348+00	347.5	0.0	2	0.4
232.5	93-08-26	gal. 348+00	347.5	0.0	12	2.6
302.0	93-09-07	N Cyg 1992	89.1	7.8	2	0.5
302.3	93-09-09	GX 1+4	1.4	9.3	12	2.6
303.0	93-09-21	GRS 1009−45	277.2	12.8	1	0.2
303.2	93-09-22	N Cyg 1992	89.1	7.8	9	2.3
303.4	93-10-01	pre-reboost	64.3	25.3	3	-.-
303.5	93-10-04	reboost				
303.7	93-10-17	N Cyg 1992	89.1	7.8	2	0.5
304.0	93-10-19	Virgo 278+67	278.2	66.7	6	1.7
305.0	93-10-25	Virgo 278+63	277.7	62.7	8	2.2
306.0	93-11-02	Virgo 278+59	277.6	58.7	7	1.8
307.0	93-11-09	Virgo 269+69	268.7	69.2	7	1.8
308.0	93-11-16	Virgo 283+75	283.2	74.7	3	1.1
308.3	93-11-19	reboost				
308.6	93-11-23	Virgo 283+75	283.2	74.7	8	3.0
310.0	93-12-01	Geminga	195.1	4.3	12	2.4
311.0	93-12-13	Virgo 284+75	283.7	74.5	2	0.6
311.3	93-12-15	reboost				
311.6	93-12-17	Virgo 284+75	283.7	74.5	3	0.9
312.0	93-12-20	Virgo 281+71	280.5	70.7	7	2.0
313.0	93-12-27	Virgo 289+79	289.3	78.7	7	2.1
314.0	94-01-03	gal. 304−01	304.2	−1.0	13	3.6
315.0	94-01-16	gal. 304−01	304.2	−1.0	7	1.8
316.0	94-01-23	Centaurus A	309.5	19.4	9	2.4
318.1	94-02-01	Cyg X−1	68.4	−0.4	7	2.0
321.1	94-02-08	1A 0535+262	181.4	−2.6	7	2.7
321.5	94-02-15	1A 0535+262	181.4	−2.6	2	0.8
317.0	94-02-17	NGC 1068	158.5	−45.4	12	4.6
319.0	94-03-01	QSO 0716+714	144.0	28.0	7	1.7
320.0	94-03-08	gal. 083−45	83.1	−45.5	7	2.5
319.5	94-03-15	QSO 0716+714	146.4	26.0	7	1.9
323.0	94-03-22	gal. 357−11	356.8	−11.3	14	4.3
322.0	94-04-05	MRK 421	197.0	58.6	14	2.5
324.0	94-04-19	gal. 015+05	15.0	5.6	7	2.5
325.0	94-04-26	gal. 147−09	147.0	−9.0	14	3.6

Table 2. continued

Phase III

Viewing Period	start (yy-mm-dd)	Z-axis pointing	galactic LONG	galactic LAT	duration (days)	eff. COMPTEL observing time (days)
326.0	94-05-10	NGC 3227	195.9	58.3	7	2.7
327.0	94-05-17	gal. 083−50	82.9	−49.6	7	2.0
328.0	94-05-24	PSR 1951+32	64.9	−0.0	7	1.8
329.0	94-05-31	gal. 253−42	253.4	−42.0	7	1.7
331.0	94-06-07	PSR 1951+32	64.9	−0.0	3	1.1
330.0	94-06-10	gal. 018+00	18.0	0.0	4	1.4
331.5	94-06-14	PSR 1951+32	64.9	−0.0	4	1.6
332.0	94-06-18	gal. 018+00	18.0	0.0	17	6.1
333.0	94-07-05	PSR 1951+32	64.9	−0.0	7	2.2
335.0	94-07-12	gal. 253−42	253.4	−42.0	6	1.5
334.0	94-07-18	gal. 009−08	9.0	−8.4	7	2.1
335.5	94-07-25	gal. 253−42	253.4	−42.0	7	1.8
336.0	94-08-01	gal. 088−47	88.4	−46.8	3	1.2
336.5	94-08-04	GRO J1655−40	340.4	2.9	5	1.5
337.0	94-08-09	PKS 0528+134	205.0	13.0	20	6.2
338.0	94-08-29	GRO J1655−40	345.0	2.5	2	0.6
338.5	94-08-31	Vela Pulsar	263.6	−2.7	20	5.6
339.0	94-09-20	3C 317	4.1	40.4	14	4.8
	93-10-04	end of Phase III				
401.0	94-10-04	Cas A	113.9	6.2	14	3.8
402.0	94-10-18	GPlane 310	310.3	−5.0	7	1.6
402.5	94-10-25	GPlane 310	306.7	−3.8	7	1.6
403.0	94-11-01	Her X−1	58.2	37.5	8	2.1
403.5	94-11-09	OJ 287	206.8	35.8	6	1.6
404.0	94-11-15	S Gal. Pole	7.2	−73.4	14	4.2
405.0	94-11-29	3C 279	306.7	56.5	9	3.2
405.5	94-12-07	GRO J1655−40	306.7	56.5	6	2.1
406.0	94-12-13	Virgo	336.3	67.2	7	2.4
407.0	94-12-20	Virgo	334.3	63.0	14	4.1
408.0	95-01-03	3C 279	305.1	57.1	7	2.0
409.0	95-01-10	LMC	274.7	−39.2	14	3.9
410.0	95-01-24	gal. 082−33	82.2	−32.6	21	5.7
411.1	95-02-14	QSO 0716+714	145.1	23.9	7	2.1
411.5	95-02-21	QSO 0716+714	143.3	22.7	7	2.1
412.0	95-02-28	Anticenter	185.3	0.7	7	2.1
413.0	95-03-07	Anticenter	191.8	−3.4	14	4.2
414.0	95-03-21	Vela	281.4	−13.5	8	1.5
414.3	95-03-29	GRO J1655−40	347.3	0.6	7	2.0
419.1	95-04-04	Orion	207.4	−19.1	7	2.5
415.0	95-04-11	LMC	275.7	−24.0	14	3.5
418.0	95-04-25	MRK 421	158.1	65.8	14	4.2
419.5	95-05-09	Orion	211.9	−17.6	14	4.5
420.0	95-05-23	Orion	198.2	−18.3	14	5.0
421.0	95-06-06	Gal. Center	355.3	0.4	7	2.2
422.0	95-06-13	Gal. Center	355.4	−0.4	7	2.1
423.0	95-06-20	Gal. Center	2.6	−0.2	10	3.2
423.5	95-06-30	PKS 1622−297	345.7	13.5	10	2.8
424.0	95-07-10	Cen A	312.7	19.0	15	4.2
425.0	95-07-25	gal. 137−47	137.4	−47.3	14	5.0
426.0	95-08-08	Anticenter	184.5	−5.9	14	3.8
427.0	95-08-22	gal. 154−10	153.8	−10.0	16	5.1
428.0	95-09-07	S Gal. Pole	270.6	−82.5	13	3.9
429.0	95-09-20	gal. 018+04	18.3	4.0	7	2.4
429.5	95-09-27	GRO J2058+42	86.3	−12.5	6	2.1
	95-10-03	end of Phase IV / Cycle-4				
501.0	95-10-03	gal. 028+04	28.0	3.6	14	4.8
502.0	95-10-17	PKS 0528+134	190.7	−11.5	14	4.9
505.0	95-10-31	Cas A−4	118.0	−2.0	7	2.4
506.0	95-11-07	Cas A−1	111.0	5.0	7	2.5
503.0	95-11-14	Cas A−3	104.0	-2.0	7	2.2
504.0	95-11-21	Cas A−2	111.0	−10.0	7	2.2
507.0	95-11-28	CTA 102	77.4	−38.6	9	2.5
507.5	95-12-07	CTA 102	77.4	−38.6	7	2.0
508.0	95-12-14	gal. 005+00	6.5	−0.2	6	1.7

Table 2. continued

Phase IV/Cycle-4

Viewing Period	start (yy-mm-dd)	Z-axis pointing	galactic LONG	galactic LAT	duration (days)	eff. COMPTEL observing time (days)
509.0	95-12-20	gal. 021+14	21.6	13.1	13	3.8
510.0	96-01-02	Monoceros	231.0	3.7	3	0.8
510.5	96-01-05	Monoceros	229.0	3.5	9	2.5
511.0	96-01-16	3C 273	298.3	62.9	14	4.9
511.5	96-01-30	3C 273	310.6	53.2	7	2.5
513.0	96-02-06	PKS 2155−304	17.6	−52.1	7	2.0
514.0	96-02-13	gal. 060−60	62.3	−60.6	7	2.4
515.0	96-02-20	QSO 1219+285	159.4	82.9	14	3.8
517.0	96-03-05	PKS 0208−512	276.8	−59.6	13	3.5
516.1	96-03-18	GRO J1655−40	341.1	5.6	3	0.8
516.5	96-03-21	MRK 501	61.0	41.2	13	4.7
518.5	96-04-03	0716+714	144.0	28.0	20	5.4
519.0	96-04-23	3C 345	63.0	40.0	14	5.0
520.0	96-05-07	Orion −1	208.8	−4.6	14	4.9
520.4	96-05-21	PKS 2155−304	17.7	−52.3	7	2.0
521.0	96-05-28	GRO J0516−609	275.6	−36.3	14	3.2
522.0	96-06-11	Cen X−3	285.7	−1.5	3	0.8
522.5	96-06-14	Cyg X−1	65.8	2.7	11	3.1
523.0	96-06-25	Orion −2	207.1	−21.0	14	4.5
524.0	96-07-09	GX 339−4	343.1	−3.6	14	3.8G
525.0	96-07-23	gal. 340−49	338.8	−54.5	7	1.4
526.0	96-07-30	Geminga	187.7	−3.6	14	3.8
527.0	96-08-13	Crab −1	190.1	−1.8	7	2.1
528.0	96-08-20	Crab −2	185.9	−0.2	7	2.4
529.5	96-08-27	GRO J1655−40	345.0	2.5	10	2.7
530.0	96-09-06	GRO J0004+73	124.7	6.4	27	8.4
531.0	96-10-03	PSR B1055−52	283.8	−0.2	11	2.4
	96-10-15	end of Phase IV / Cycle-5				
601.1	96-10-15	PSRJ2043+274	70.1	−10.5	14	4.9
520.9	96-10-29	Orion −1	214.4	3.2	14	4.5
602.0	96-11-12	GAL 60+65	60.0	65.0	7	2.4
603.0	96-11-19	GAL 60+65	60.0	65.0	7	2.5
605.1	96-11-26	GAL 43+57	43.2	56.8	7	2.5
604.1	96-12-03	GAL 48+61	48.4	60.7	7	2.4
606.0	96-12-10	3C 279	306.4	56.4	7	2.2
607.0	96-12-17	3C 279	306.5	56.4	6	1.7
608.0	96-12-23	3C 279	306.8	56.7	7	1.9
609.0	96-12-30	3C 279	306.9	56.8	8	2.4
610.0	97-01-07	3C 279	306.9	56.8	7	2.3
610.5	97-01-14	3C 279	306.6	58.9	7	2.5
611.1	97-01-21	3C 279	306.9	56.8	7	2.5
612.1	97-01-28	Cyg X−1	71.3	3.1	7	2.0
624.1	97-02-04	GAL 16+00	15.9	3.4	7	2.0
614.5	97-02-11	GAL 40−60	39.8	−60.3	7	2.0
616.1	97-02-18	PKS 0528+134	191.4	−11.0	28	8.1
617.1	97-03-18	Orion −3	220.0	−5.0	6	2.0
617.2	97-03-24	Reboost Test			1	
617.3	97-03-25	Orion −3	220.0	−5.0	1	0.3
617.4	97-03-26	Reboost Test			1	
617.5	97-03-27	Orion −3	220.0	−5.0	5	1.7
617.6	97-04-01	Reboost (1)			6	
617.7	97-04-07	Orion −3	220.0	−5.0	2	0.7
617.8	97-04-09	MRK 501	66.8	37.3	6	1.8
618.0	97-04-15	Carina −2	274.3	−3.0	21	5.5
619.0	97-05-06	Cir X−1	319.6	−1.6	8	2.1
619.2	97-05-14	GRS 1915	47.3	−0.9	6	1.8
619.4	97-05-20	Cir X−1	319.6	−1.6	28	7.3
619.5	97-05-28	Reboost (2)			7	
619.7	97-06-04	Cir X−1	319.6	−1.6	6	1.6
620.0	97-06-10	GAL 16+4	15.8	3.6	7	2.4
621.5	97-06-17	3C 279	301.7	57.8	7	2.5

Table 2. continued

Phase IV/Cycle-6

Viewing Period	start (yy-mm-dd)	Z-axis pointing	galactic LONG	galactic LAT	duration (days)	eff. COMPTEL observing time (days)
622.0	97-06-24	Orion −1	226.6	−21.3	21	6.7
623.5	97-07-15	BL Lac	92.6	−10.4	7	2.5
623.0	97-07-22	Orion −2	207.5	−28.4	14	4.3
625.0	97-08-05	GRS 1758−258	1.4	0.8	14	4.3
615.1	97-08-19	PKS 1622−297	348.8	13.3	7	2.1
626.0	97-08-26	GAL 270−75	270.0	−75.0	7	2.0
627.0	97-09-02	PSR 1055−52	288.1	2.0	7	1.9
628.0	97-09-09	GAL 300−74	300.2	−74.3	7	1.8
629.0	97-09-16	GAL 300−74	300.2	−74.3	7	2.0
630.0	97-09-23	PSR 1055−52	288.1	2.0	14	3.2
632.1	97-10-07	Carina −1	307.9	−7.5	27	5.9
631.0	97-11-03	PKS 0235+164	156.8	−39.1	8	2.4
	97-11-11	End of Phase IV/Cycle-6				
701.0	97-11-11	PKS 2155−304	10.1	−54.1	7	2.1
702.0	97-11-18	PKS 2155−304	10.1	−54.1	7	2.2
703.0	97-11-25	GAL 035+20	34.9	19.3	7	2.5
704.0	97-12-02	GAL 035+20	34.6	13.9	7	2.4
705.0	97-12-09	PSR B1509−58	319.6	7.8	7	2.0
706.0	97-12-16	PSR B1509−58	320.4	3.5	7	2.0
707.0	97-12-23	PSR B1509−58	316.9	−0.2	7	1.9
708.0	97-12-30	PKS 2155−304	10.1	−54.1	7	2.1
709.1	98-01-06	PKS 2155−304	10.1	−54.1	7	2.1
710.0	98-01-13	J1835+5919	85.9	29.4	8	3.0
711.0	98-01-21	J1835+5919	85.9	29.4	6	2.1
712.0	98-01-27	GAL 035+20	32.8	20.3	28	8.4
713.0	98-02-24	GAL 110−20	108.8	−24.6	14	5.0
714.0	98-03-10	GAL 350−70	39.7	−72.3	7	2.2
715.0	98-03-17	GAL 350−70	57.3	−73.6	3	0.9
715.5	98-03-20	1156+295	189.6	78.2	7	2.8
716.5	98-03-27	MRK 421	176.6	61.8	6	2.1
716.7	98-04-02	MRK 421	177.9	63.8	12	4.2
717.0	98-04-14	Cen X−3	289.1	−3.7	9	2.4
718.0	98-04-22	Cen X−3	287.8	2.5	7	1.9
719.0	98-04-29	Cen X−3	292.1	0.3	6	1.7
720.5	98-05-05	GRS 1915+105	44.6	0.4	10	3.5
721.0	98-05-15	MRK 501	63.6	38.9	4	1.4
721.5	98-05-19	SN 1998bu	234.4	57.0	3	1.1
722.5	98-05-22	MRK 501	63.6	38.9	5	1.5
723.5	98-05-27	SN 1998bu	230.1	55.2	6	2.1
725.5	98-06-02	SN 1998bu	230.2	55.2	14	4.9
726.5	98-06-16	SN 1998bu	230.2	55.1	7	2.5
727.5	98-06-23	Vela pulsar	269.0	−3.0	7	2.0
727.7	98-06-30	SN 1998bu	239.0	58.8	7	2.0
724.5	98-07-07	Geminga	191.5	0.8	14	5.0
728.5	98-07-21	SN 1998bu	231.6	55.8	35	11.2
728.1	98-08-21	aspect lost			4	
728.2	98-08-25	aspect tests			1	
730.6	98-08-26	SN 1998bu	254.9	45.5	14	4.6
731.5	98-09-08	SN 1998bu	235.7	55.4	7	2.2
732.5	98-09-15	GAL 058−12	232.3	58.7	7	2.5
728.7	98-09-22	J0218+4232	139.4	−18.7	3	1.1
729.5	98-09-25	J1550−564	324.9	−0.2	11	3.0
734.0	98-10-06	GAL 190−70	204.1	−72.0	14	4.5
728.9	98-10-13	J0218+4232	139.4	−18.7	21	6.1
734.5	98-11-03	GAL 190−70	204.1	−72.0	14	4.6
736.0	98-11-10	Orion B1	227.9	−4.3	6	1.9
736.5	98-11-16	Leonid Save	17.3	−37.5	2	
736.7	98-11-18	Orion B1	227.9	−4.3	6	1.9
737.0	98-11-24	GAL 044−09	44.3	−9.1	7	2.6
	98-12-01	End of Phase IV/Cycle-7				

Table 3. Spin-down pulsars

Pulsar	l [deg.]	b [deg.]	P [ms]	$\dot{P}$ [10^{-15}]	d [kpc]	Phase Averaged Flux (10^{-5} cm^{-2} s^{-1}) $(0.75-1)$ [MeV]	$(1-3)$ [MeV]	$(3-10)$ [MeV]	$(10-30)$ [MeV]	Other energy ranges [MeV]	VP or Phase	Ref.
PSR B1951+32	68.77	2.82	39.53	5.849	2.5	2.3 ± 1.4					Phase I–IV/Cycle-6	6
PSR B0531+21 (Crab)	184.56	−5.78	33.34	421.2	2.0	16.6 ± 3.0			1.5 ± 0.5	$18.4 \pm 2.2(1.0-1.6$ MeV) $6.5 \pm 1.2(1.6-2.1$ MeV) $5.6 \pm 1.1(2.36-4.0$ MeV) $1.6 \pm 0.6(4.0-5.6$ MeV) $1.9 \pm 0.5(5.6-10$ MeV)	Phase I–IV/Cycle-5	1,2
PSR J0633+1746 (Geminga)	195.13	4.65	237.1	10.98	0.16	-2.7 ± 1.5	$+3.2 \pm 2.2$	$+2.4 \pm 1.1$	-0.1 ± 0.4		Phase I–III	3
PSR B0656+14	201.11	8.26	384.87	55.03	0.77	0.0 ± 1.9	-0.9 ± 2.3	-0.7 ± 1.2	0.8 ± 0.6		Phase I–IV	4
PSR B833 − 45 (Vela)	263.55	−2.79	89.29	124.3	0.5	3.6 ± 1.9	2.8 ± 2.2	2.9 ± 1.0	2.3 ± 0.4		Phase 0 + I	5,7
PSR B1055 − 52	286.0	6.6	197.1	5.8	1.5	1.8 ± 0.5^{d}					Phase I–IV/Cycle-6	8
PSR B1509 − 58 (Circinus)	320.32	−1.16	150.65	1537	4.4.	8.3 ± 1.7		3.2 ± 0.6	0.2 ± 0.2^{a} 0.7 ± 0.2^{b} 1.1 ± 0.2^{c}		Phase I–IV/Cycle-6	9,10

Notes

(a) Flux main pulse from timing analysis. (b) Flux main pulse above background from spatial analysis. (c) Total flux from spatial analysis. (d) Note that the flux given in ref. (8) should be in units ph cm^{-2} s^{-1} MeV^{-1}.

References

(1) Much et al. (1995a)
(2) Much et al. (1997)
(3) Kuiper et al. (1996)
(4) Hermsen et al. (1997)
(5) Schönfelder et al. (1995)
(6) Kuiper et al. (1998a)
(7) Kuiper et al. (1998b)
(8) Thompson et al. (1999)
(9) Kuiper et al. (1999a)
(10) Kuiper et al. (1999b)

Table 4. Galactic sources $|b| < 10°$

Source	Position l [deg]	Position b [deg]	Fluxes[a] (10^{-5} photon cm^{-2} s^{-1}) $(0.75-1)$ [MeV]	$(1-3)$ [MeV]	$(3-10)$ [MeV]	$(10-30)$ [MeV]	Other Energy Ranges [MeV]	Spect. Fits	VP or Phase	Notes	Ref.
GRO J 1823 − 12 (2 EG J 1825 − 1307)	18.5	−0.5	4.1 ± 1.7	9.9 ± 1.5	3.5 ± 0.6	1.0 ± 0.2		f	VP 1 to 522.5	c	(9)
Cygnus X − 1	71.3	3.1				< 1.39	11.9 ± 3.0 (0.75 − 0.85) 9.5 ± 2.2 (0.85 − 1) 16.7 ± 2.7 (1 − 2) 6.9 ± 1.6 (3 − 5) < 1.15 (5 − 10)	a	Phase I to III (up to VP 318.1)	b	(3) (3a)
GRO J 2227+61 (2 EG 2227+61) (2CG 106+1.5)	106.6	3.1	12.6 ± 4.5	30.8 ± 5.5	≤ 6.3	≤ 1.48		e	VP 2+7+34		(6)
GT 0236+610 (2EG J0241+6119) (2CG 135+01)	135.7	1.1	< 4.8 < 4.8	11.2 ± 3.2 5.6 ± 3.0	5.0 ± 1.2 3.2 ± 1.3	1.24 ± 0.38 < 1.3		b	VP 15+31+34+211 +319+325	b c	(5)
Nova Per 1992 (GRO J0422+32)	165.9	−11.9	< 35.0 27.5 ± 10.00		< 11.9 < 6.0	< 2.8 < 2.2	28.0 ± 10.0 (1 − 2) < 8.1 (2 − 3) < 15.0 (1 − 2) < 6.6 (2 − 3)	c	VP 36.5 VP 39	b	(4)
Crab Unpulsed	184.6	−5.8					34.07 ± 1.57(0.78 − 0.96) 31.11 ± 1.30(0.96 − 1.16) 21.54 ± 1.09(1.16 − 1.38) 18.68 ± 1.04(1.38 − 1.62) 13.03 ± 0.82(1.62 − 1.88) 8.90 ± 0.71(1.88 − 2.16) 7.84 ± 0.70(2.16 − 2.48)		Phase I to IV/Cycle-5	a,b	

Table 4. continued

Source	Position l [deg]	Position b [deg]	Fluxes[a] (10^{-5} photon cm^{-2} s^{-1}) $(0.75-1)$ [MeV]	$(1-3)$ [MeV]	$(3-10)$ [MeV]	$(10-30)$ [MeV]	Other Energy Ranges [MeV]	Spect. Fits	VP or Phase	Notes	Ref.
Crab Unpulsed cont.							$8.66 \pm 0.57 (2.48-2.84)$ $6.14 \pm 0.52 (2.84-3.22)$ $4.41 \pm 0.46 (3.22-3.62)$ $4.28 \pm 0.41 (3.62-4.08)$ $4.44 \pm 0.36 (4.08-4.56)$ $2.94 \pm 0.33 (4.56-5.08)$ $3.42 \pm 0.32 (5.08-5.66)$ $2.30 \pm 0.28 (5.66-6.26)$ $2.15 \pm 0.28 (6.26-6.94)$ $1.60 \pm 0.25 (6.94-7.64)$ $1.17 \pm 0.20 (7.64-8.42)$ $1.36 \pm 0.17 (8.42-9.26)$ $1.24 \pm 0.15 (9.26-10.16)$ $1.05 \pm 0.15 (10.00-11.20)$ $1.12 \pm 0.14 (11.20-12.48)$ $1.12 \pm 0.14 (12.48-13.92)$ $0.62 \pm 0.13 (13.92-15.52)$ $0.83 \pm 0.14 (15.52-17.28)$ $0.50 \pm 0.14 (17.28-19.28)$ $0.31 \pm 0.14 (19.28-21.60)$ $0.23 \pm 0.15 (21.60-24.08)$ $0.16 \pm 0.18 (24.08-26.88)$ $0.13 \pm 0.27 (26.88-30.00)$				(1),(2) (7)
Vela/Carina	273°	-6°	< 6.0	< 5.4	7.5 ± 1.1	< 1.1			VP 1 to 522.5	a,c,d	(8)

Spectral Fits

a. Wien spectrum with $kT \sim 190$ keV; for fits to 1991 data only see McConnell et al. (1994).
b. $1.75\ 10^{-4}(E/1\ \mathrm{MeV})^{-1.95}$ photon cm^{-2} s^{-1} MeV^{-1} (Ref. 5).
c. See ref. 4.
d. $(1.12 \pm 0.03) \cdot 10^{-4}(E/3.5\ \mathrm{MeV})^{-(2.02\pm0.03)}$ photon cm^{-2} s^{-1} MeV^{-1} < 10 MeV (Ref. 7).
e. Power-law spectrum $\sim E^{-\alpha}$, with $\alpha = 2.20 \pm 0.14$.
f. Power-law spectrum $\sim E^{-\alpha}$, with $\alpha = 2.0$.

Notes

a. Flux values with statistical 1 σ uncertainties and 2 σ upper limits are given.
b. No model for Galactic diffuse emission is included in this analysis.
c. Model for Galactic diffuse emission is included.
d. The excess is extended and can be explained by a 2-source model with sources at (273.8, −3.5) and (271.9, −9.0).

References

(1) Much et al. (1995a)
(2) Much et al. (1995b)
(3) McConnell et al. (1997b)
(3a) McConnell et al. (1994)
(4) van Dijk et al. (1995)
(5) van Dijk (1996)
(6) Iyudin et al. (1997b)
(7) van der Meulen et al. (1998)
(8) van der Meulen et al. (1999)
(9) Bloemen et al., in preparation

Table 5. Active galactic nuclei

Source	Z-Value	Position		Flux (10^{-5} photon cm^{-2} s^{-1})				VP or Phase	Ref.
		l [deg]	b [deg]	$(0.75-1)$ [MeV]	$(1-3)$ [MeV]	$(3-10)$ [MeV]	$(10-30)$ [MeV]		
CTA 102 (PKS 2230+114)	1.037	77.4	−38.6	< 10.4	< 12.1	< 7.4	1.4 ± 1.1	VP 19	(1)
				< 15.1	< 24.7	< 10.7	< 6.9	VP 26+28	
				< 17.9	< 30.0	< 13.5	< 6.5	VP 37	
				< 7.8	< 12.2	< 6.4	1.9 ± 0.9	Phase 1	
3C 454.3 (PKS 2251+15)	0.859	86.1	−38.2	< 10.5	< 12.9	6.9 ± 3.3	< 3.8	VP 19	(1)
				< 17.5	< 23.0	< 8.1	6.1 ± 1.80	VP 26+28	
				< 20.2	12.4 ± 10.4	< 13.0	2.2 ± 1.8	VP 37	
				< 10.4	< 9.2	2.8 ± 2.3	2.9 ± 1.0	Phase 1	
PKS 0528+134 (OG 147)	2.06	191.4	−11	9.4 ± 8.2	9.7 ± 6.3	4.4 ± 2.5	3.2 ± 1.0	VP 0	
				16.6 ± 8.7	< 13.8	< 7.7	3.0 ± 1.0	VP 1	
				< 16.2	< 21.8	< 9.4	< 3.2	VP 2.5	
				< 15.6	< 18.7	< 8.4	< 2.8	VP 36/39	
				< 32.1	15.3 ± 12.3	$< 15.2 \pm 4.7$	3.3 ± 1.7	VP 213	
				< 24.4	$< 14.0 \pm 9.5$	$< 4.4 \pm 3.6$	< 2.7	VP 221	
				< 20.9	< 17.4	5.0 ± 3.6	< 4.3	VP 310	
				11.3 ± 10.0	18.1 ± 8.3	< 6.3	< 3.1	VP 321	(2)
				23.8 ± 7.9	20.6 ± 6.6	< 5.0	< 1.8	VP 337	
				< 32.1	15.3 ± 12.3	15.2 ± 4.7	3.3 ± 1.7	VP213	
				< 8.7	5.8 ± 3.4	4.3 ± 1.4	2.0 ± 0.5	Phases I+II	
				4.2 ± 3.4	8.5 ± 2.7	2.3 ± 1.0	1.3 ± 0.4	Phases I–III	
GRO J0516−609 (PKS 0506−612/ PKS 0522−611)		270	−35	< 12.8	< 18.1	< 8.3	< 2.1	VP 6	(3)
				< 18.6	20.0 ± 7.2	< 12.4	< 4.2	VP 10	
				< 11.0	9.2 ± 6.2	8.9 ± 3.2	< 1.7	VP 17	
				< 9.4	15.1 ± 4.6	5.7 ± 2.5	< 1.5	VP 10+17	
PKS 0208−512 (RX J02107−5100)	1.003	276.1	−61.8		21 ± 9			VP 6	
					< 26			VP 9	
					< 15			VP 10	
					< 18			VP 13.5	
					< 23			VP 17	(4)
					35 ± 12			VP 220	
					44 ± 9			VP 224	
				< 12	41 ± 7	< 7	< 3	Phase II	
3C 273 (1226+023)	0.158	290.0	64.4	25.9 ± 6.2 (0.75–8 MeV)		< 1.7 (8–30 MeV)		VP 3	(5)
				13.8 ± 4.8 $(0.75-1.25)$	10.7 ± 3.7 $(1.25-3)$	5.6 ± 1.9 $(3-8)$	< 1.7 $(8-30)$	VP 3	
				< 19.2 (0.75–8 MeV)		< 2.5 (8–30 MeV)		VP 11	
				< 8.5	14.5 ± 2.2	3.9 ± 0.9	0.6 ± 0.3	Phases I to III	(6)
GRO J1224+2155 (PKS 1222+216)		255.1	+81.7	< 4.8	< 5.4	2.6 ± 0.9	< 0.9	Phases I–III	(6)
3C 279 (1253−055)	0.538	305.1	57.1	< 13.8 $(0.75-8$ MeV)		2.9 ± 0.9 $(8-30$ MeV)		3	(5)
				< 12.1 $(0.75-8$ MeV)		< 3.2 $(8-30$ MeV)		1	
				< 8.8	6.3 ± 2.0	< 3.2	0.8 ± 0.3	Phases I to III	(6)
				5.9 ± 3.0	6.9 ± 2.4	1.5 ± 1.0	1.0 ± 0.3	Phases I to IV	(9)

Table 5. continued

Source	Z-Value	Position		Flux (10^{-5} photon cm^{-2} s^{-1})				VP or Phase	Ref.
		l [deg]	b [deg]	$(0.75-1)$ [MeV]	$(1-3)$ [MeV]	$(3-10)$ [MeV]	$(10-30)$ [MeV]		
Centaurus A	~ 3 Mpc	309.5	19.4	16.4 ± 8.1	< 17.6	4.0 ± 2.4	1.6 ± 0.8	VP 12	(7)
NGC 5128				31.0 ± 12.0	16.4 ± 11	< 9.2	< 5.8	VP 14[a]	
				16.8 ± 16.0	< 28.6	< 15.8	< 2.9	VP 23[b]	
				< 20.1	30.3 ± 13.0	7.1 ± 6.2	< 3.9	VP 27	
				< 20.5	< 35.0	< 14.9	< 5.7	VP 32	
				14.1 ± 5.2	10.8 ± 4.5	2.2 ± 1.9	< 1.4	Phase I	
				< 12.2	< 14.3	8.8 ± 2.6	1.3 ± 0.9	VP 207	
				18.8 ± 15.0	14.5 ± 12.0	5.1 ± 4.4	< 3.8	VP 208	
				< 23.3	21.3 ± 8.3	10.8 ± 3.1	< 1.7	VP 215 +217	
				< 11.9	5.8 ± 4.6	8.6 ± 1.8	< 1.7	Phase II	
Centaurus A				28.1 ± 9.9	< 26.6	< 6.7	2.3 ± 1.4	VP 314	
(NGC 5128)				< 6.9	4.5 ± 2.9	< 2.2	< 2.4	VP 315	
				< 30.6	< 17.1	< 9.0	< 1.6	VP 316	
				24.1 ± 6.2	< 14.9	< 3.9	< 1.2	Phase III	
				18.7 ± 14.0	< 36.1	< 9.1	< 3.0	VP 402.0	
				< 28.7	26.6 ± 12.0	< 8.9	< 4.2	VP 402.5	
				< 13.5	18.6 ± 7.7	3.6 ± 2.7	< 1.3	VP 424.0	
				< 15.2	21.9 ± 5.8	< 4.5	< 1.1	Phase IV	
				9.1 ± 3.0	6.4 ± 2.5	2.1 ± 1.0	< 0.6	Phases I to IV	
PKS 1622−297	0.815	348.5	13.5	< 22.0	< 13.5	< 6.1	3.3 ± 0.7	VP 421 − 423.5	(8)

Notes

[a]Heavily influenced by Earth in field-of-view.
[b]Large data loss due to malfunctioning tape recorder.

References

(1) Blom et al. (1995a)
(2) Collmar et al. (1997a)
(3) Bloemen et al. (1995)
(4) Blom et al. (1995b)
(5) Williams et al. (1995b)
(6) Collmar et al. (1996)
(7) Steinle et al. (1998)
(8) Collmar et al. (1997b)
(9) Collmar et al. (1997c)

Table 6. Unidentified high-latitude source

Source	COMPTEL Position l [deg]	b [deg]	Flux (10^{-5} cm^{-2} s^{-1}) $(0.75-1)$ [MeV]	$(1-3)$ [MeV]	$(3-10)$ [MeV]	$(10-30)$ [MeV]	Other Energy Ranges [MeV]	VP/Phase	Ref.
GRO J 1753+57[a]	85.5	30.5	< 13.9	< 14.0	< 13.5	< 2.4		VP 2	(1)
			< 17.9	< 13.8	< 7.2	< 2.8		VP 9.5	(6)
			< 24.7	48.9 ± 9.1	< 12.2	< 2.2		VP 201	
			18.6 ± 9.9	28.8 ± 9.4	< 12.1	< 4.9		VP 202	
			< 7.0	< 8.8	5.6 ± 2.7	< 2.8		VP 203	
			< 9.4	11.0 ± 5.1	< 8	< 2.0		VP 212	
GRO J 1040+48	165	57				< 0.56	$19.8 \pm 3.2(0.75-1.36)$	Phases I - II	(2)
							$6.48 \pm 1.08(1.56-2.1)$		
							$1.97 \pm 1.6(2.3-4.0)$		
							< 2.58 $(4-10)$		
							$24 \pm 3(0.75-3)$	Phases I - II	
							$7 \pm 4(0.75-3)$	Phases III - IV	
GRO J 1214+06	278.9	+66.6	< 5.1	< 6.8	4.0 ± 0.9	< 0.7		Phases I - III	(3)
Extended emission from the HVC complexes M and A area[b]	$145 < l < 195$	$35 < b < 65$					$150 \pm 10(0.75-3)$	Phases I to IV	(4)
Extended emission from the HVC complex C area[c]	$75 < l < 95$	$25 < b < 45$					$110 \pm 10(0.75-3)$	Phases I to IV	(5)

[a]The emission cannot arise from a single source, but it can be modelled as a combination of emission from both GRO J1837+59 (a bright unidentified EGRET source), and the steep spectrum EGRET blazar QSO 1739+522.
[b]Cloud region contains: 2EG J0917+4420, 2EG J0957+5515, GRO J1040+48.
[c]Cloud region contains: GRO J1753+57, 2EG J1739+5152, 2EG 1731+6007, 2EG J 1835+5913.

References

(1) Williams et al. (1995a)
(2) Iyudin et al. (1996)
(3) Collmar et al. (1996)
(4) Blom et al. (1997b)
(5) Blom et al. (1997a)
(6) Williams et al. (1999)

Table 7. Gamma-ray line sources

Name	Position l [deg]	Position b [deg]	Line Energy [MeV]	Flux [10^{-5} photons cm^{-2} s^{-1}]	VP or Phase	Note	Ref.
SN 1991T	292.61	65.19	0.847	5.3 ± 2.0	VP 3.0, 11.0, 204.0, 205.0, 206.0		
			1.238	3.6 ± 1.4			(1)
			both combined	8.9 ± 3.4			
Cas A	111.7	-2.1	1.157	4.2 ± 0.9	VP 34.0, 211.0, 302.0, 303.2, 303.7, 401.0	possibly broadened line result from all obs. up to 401	(2) (3)
				3.4 ± 0.9	Phases I to III		(7)
SNR G266.5 − 1.5	266.5	-1.5	1.157	3.8 ± 0.7	Phases I to IV/ Cycle-6 (VP 617.1)		(8)
Inner Galaxy	$-32 < l < 35$	$-5 < b < 5$	1.809	28.0 ± 1.5	Phases I to IV/ Cycle-5	emission extended beyond this region	(4)
Vela Region	$257 < l < 273$	$-5 < b < 5$	1.809	2.9 ± 0.6	Phases I to IV / Cycle-5	possibly extended emission (few deg.)	(4)

Table 7. continued

Name	Position l [deg]	Position b [deg]	Line Energy [MeV]	Flux [10^{-5} photons cm^{-2} s^{-1}]	VP or Phase	Note	Ref.
Cygnus Region	$73 < l < 93$	$-7 < b < 7$	1.809	7.0 ± 1.4	VP 2.0, 7.0, 34.0 203.×, 212.0, 302.0, 303.×, 318.1, 328.0, 331.×, 333.0	extended source	(5)
Cygnus Superbubble	$73 < l < 87$	$-7 < b < +7$	1.809	4.6 ± 1.1	see Cygnus region	extended source	(5)
Carina Region	286.5	0.5	1.809	2.7 ± 0.6	Phases I to IV/ Cycle-5	point-like source	(4)
Perseus/Cas-Tau Region	$125 < l < 168$	$-17 < b < 28$	1.809	8.4 ± 1	Phases I to IV/ Cycle-5	low level extended emission	(4)
Neutron capture source	300	-30	2.223	3.3 ± 0.9	VP 1.0 to VP 523.0	white dwarf RE J0317 − 853 as possible source candidate	(6)

References

(1) Morris et al. (1995)
(2) Iyudin et al. (1994)
(3) Schönfelder et al. (1996)
(4) Oberlack (1997)
(5) del Rio et al. (1996)
(6) McConnell et al. (1997a)
(7) Dupraz et al. (1997)
(8) Iyudin et al. (1998)

Table 8. Gamma-ray burst source locations

Burst	COMPTEL Location			Accum. Time	$(0.75-30)$ [MeV] Fluence	Detect. Signif.	Spectral Fit in Telescope Mode[a]		Variability of Spect. in Single Det. Mode	References
	l [deg]	b [deg]	Error Radius[b] [deg]	[s]	[10^{-5} erg cm^{-2}]	σ	A [ph cm^{-2} s^{-1} MeV^{-1}]	α		
GRB 910425	228.1	−20.6	0.92	39.27	9.07	5.7	0.29 ± 0.04	1.8 ± 0.18	yes (> 0.6 MeV)	1, 2, 7, 17, 20, 22, 23, 24
GRB 910503	172.0	+5.4	0.44	57.34	13.90	12.8	0.54 ± 0.05	2.19 ± 0.10	yes (> 0.6 MeV)	1, 2, 7, 17, 18, 21, 22, 23, 25, 26
GRB 910601	74.1	−5.4	0.46	19.83	3.72	14.4	1.11 ± 0.10	3.41 ± 0.18	yes (> 0.6 MeV)	1, 2, 7, 17, 20, 22, 23, 24, 26, 27
GRB 910627	315.1	+57.3	1.63	9.13	0.56	4.0	0.16 ± 0.04	2.31 ± 0.26	yes (> 0.6 MeV)	1, 2, 7, 17, 20, 22, 23, 26
GRB 910709	136.3	+36.0	1.80	0.60	0.53	5.4	4.19 ± 0.99	2.99 ± 0.48	yes (> 0.6 MeV)	1, 2, 7, 26
GRB 910814	94.7	−26.9	0.39	33.24	8.53	13.4	0.79 ± 0.06	2.46 ± 0.13	yes (> 0.6 MeV)	1, 2, 7, 17, 20, 22, 23, 24, 26
GRB 911118	273.0	+34.2	1.11	9.12	0.68	5.9	0.50 ± 0.09	3.82 ± 0.58	yes (> 0.6 MeV)	1, 2, 7, 17, 19, 26
GRB 920622	161.3	+57.9	0.81	24.17	5.74	13.5	0.91 ± 0.09	2.69 ± 0.17	yes	1, 2, 3, 6, 19
GRB 920627	263.9	+46.4	1.18	59.37	0.96	5.0	0.04 ± 0.01	2.27 ± 0.40		29, 30
GRB 920830	318.0	−20.1	1.35	4.05	0.40	5.4	0.32 ± 0.08	2.51 ± 0.35	no	1, 2, 6, 16
GRB 930118	328.4	+22.3	1.47	4.00	0.27	3.9	0.21 ± 0.07	2.46 ± 0.55	no	1, 2, 6, 16
GRB 930131	291.6	+54.4	1.77	1.02	6.83	5.1	9.32 ± 2.22	1.88 ± 0.25	yes $(1-30)$ MeV	1, 2, 6, 8, 9, 14, 15, 16
GRB 930309	96.9	+2.8	0.74	39.98	0.82	6.0	0.09 ± 0.02	2.87 ± 0.35	no	1, 2, 6, 9, 13, 16
GRB 930612	282.0	−24.4	1.60	12.83	0.77	4.1	0.11 ± 0.03	2.05 ± 0.26	no	1, 2
GRB 930704	152.5	+22.4	1.08	18.15	0.44	4.0	0.08 ± 0.02	2.54 ± 0.40	yes	1, 2, 5, 12, 28
GRB 931229	36.2	+45.1	2.35	0.60	0.39	5.0	3.65 ± 1.23	3.32 ± 0.75	no	1, 2

Table 8. continued

Burst	COMPTEL Location			Accum. Time	(0.75 − 30) [MeV] Fluence	Detect. Signif.	Spectral Fit in Telescope Mode[a]		Variability of Spect. in Single Det. Mode	References
	l [deg]	b [deg]	Error Radius [deg]	[s]	[10^{-5} erg cm^{-2}]	σ	A [ph cm^{-2} s^{-1} MeV^{-1}]	α		
GRB 940217	154.5	−55.5	0.69	162.79	17.40	18.8	0.38 ± 0.02	2.60 ± 0.07	yes (> 0.3 MeV)	1, 2, 4, 10
GRB 940301	151.6	+24.1	0.40	42.20	4.55	11.8	0.25 ± 0.02	2.22 ± 0.11	yes	1, 2, 5 11, 12 28
GRB 940314	88.0	−59.6	1.43	51.00	1.43	5.2	0.11 ± 0.02	2.72 ± 0.24	no	1, 2
GRB 940520	62.5	−31.8	0.70	30.00	2.09	6.9	0.23 ± 0.03	2.53 ± 0.18		29, 30, 31
GRB 940619	9.3	−26.3	1.15	102.00	2.92	4.6	0.07 ± 0.01	2.26 ± 0.22		29, 30, 31
GRB 940708	61.1	−4.2	1.03	12.00	0.76	7.8	0.35 ± 0.08	3.25 ±0.60		29, 30, 31
GRB 940728	243.2	−29.6	1.10	11.87	0.66	3.9	0.10 ± 0.03	2.04 ± 0.29		29, 30, 31
GRB 940921	322.3	+44.4	0.68	24.00	4.62	11.3	0.58 ± 0.06	2.44 ± 0.14		29, 30, 31
GRB 941017	53.7	−10.0	2.10	78.45	10.32	7.7	0.45 ± 0.09	2.57 ± 0.27		29, 30, 31
GRB 950208	107.6	−3.5	1.95	62.00	3.82	5.7	0.23 ± 0.02	2.66 ± 0.21		29, 30, 31
GRB 950421	272.1	−39.0	1.43	3.00	0.75	5.4	0.49 ± 0.11	2.10 ± 0.24		29, 30, 31
GRB 950425	277.8	+23.6	0.34	70.00	21.51	18.0	0.72 ± 0.05	2.23 ± 0.10		29, 30, 31
GRB 950522	197.9	+15.9	1.14	26.00	2.69	9.5	0.24 ± 0.03	2.22 ± 0.18		29, 30, 31
GRB 960808	173.5	+3.95	0.91	14	0.90	6.5	0.27 ± 0.05	2.71 ± 0.39		32
GRB 961001	137.1	−5.30	1.74	12	1.01	3.8	0.26 ± 0.06	2.36 ± 0.40		32

[a] Power-law fit: $\mathrm{d}n/\mathrm{d}E = A$ (ph cm^{-2} s^{-1} MeV^{-1}) $\cdot$ $(E/1\ \mathrm{MeV})^{-\alpha}$.
[b] The error radius is defined as the angular radius of a circle having the same area as the irregularly shaped COMPTEL 1σ confidence region.

References

1. Kippen (1995d)
2. Kippen et al. (1995c)
3. Greiner et al. (1995)
4. Winkler et al. (1995)
5. Kippen et al. (1995b)
6. Kippen et al. (1995a)
7. Hanlon et al. (1994a)
8. Ryan et al. (1994b)
9. Kippen et al. (1994c)
10. Kippen et al. (1994a)
11. Kippen et al. (1994b)
12. Ryan et al. (1994a)
13. Bennett et al. (1993)
14. Ryan et al. (1993)
15. Kippen et al. (1993)
16. Varendorff et al. (1993)
17. Winkler et al. (1993b)
18. Winkler et al. (1993a)
19. Connors et al. (1993b)
20. Connors et al. (1993a)
21. Winkler et al. (1992)
22. Varendorff et al. (1992)
23. Schönfelder (1991)
24. Collmar et al. (1993)
25. Schaefer et al. (1994)
26. Hanlon et al. (1994b)
27. Share et al. (1994)
28. Hanlon et al. (1995)
29. Kippen et al. (1996)
30. Kippen et al. (1998a)
31. Kippen et al. (1998b)
32. Connors et al. (1997)

Table 9. Solar flare detections

COMPTEL Flare No.	TJD	GOES Start time	GOES Class	BATSE Flare No.	BATSE Trigger No.	COMPTEL Int. time (s)	COMPTEL total cts	COMPTEL Peak cts	Peak BATSE cts/area	GRO mass g/cm^2
sf 910604-033651	8411	03:37	X 12.0	387	262	900	*	*	N / A	39.5
sf 910606-005900	8413	00:54	X 12.0	388	281	6845	31198	589	N / A	44.4
sf910609-013433	8416	01:37	X 10.0	419	299	5075	5880	550	N / A	22.8
sf 910611-015335	8418	02:09	X 12.0	485	319	1440	13056	565	N / A	25.8
sf 910630-025434	8437	02:43	M 5.0	665	468	600	2761	440	3.71 E+05	6.8
sf 910702-193346	8439	19:35	M 4.6	684	479	830	2158	319	4.67 E+05	6.5
sf 910717-062456	8454	06:18	X 1.1	786	544	1350	490	28	3.79 E+05	6.7
sf 910825-004153	8493	00:31	X 2.1	1140	721	837	3332	89	2.22 E+05	6.1
sf 911005-065039	8534	08:00	C 6.1	1410	N / A	812	†	†	2.2 E+03	5.1
sf 911014-173340	8543	17:34	M 6.6	1491	901	500	†	†	2.35 E+05	25.5
sf 911015-091400	8544	09:12	C 7.7	1498	904	352	343	50	2.14 E+04	24.7
sf 911024-041512	8553	05:30	X 2.1	1552	922	360	2800	681	3.5 E+03	22
sf 911027-020404	8556	02:06	X 1.9	1643	943	807	1782	142	3.35 E+05	25
sf 911027-053621	8556	05:38	X 6.1	1648	945	2000	24206	817	N / A	25
sf 911030-061616	8559	06:11	X 2.5	1723	965	2500	2463	39	2.00 E+05	24
sf 911030-191140	8559	19:13	M 4.3	1743	968	500	413	38	1.60 E+05	24
sf 911030-222354	8559	22:23	C 5.3	1749	970	236	778	46	1.95 E+04	24
sf 911115-223311	8575	22:34	X 1.5	1901	1066	876	3214	329	1.30 E+06	6.4
sf 911130-034430	8590	03:44	M 5.7	1928	1131	447	362	73	7.18 E+05	8.6
sf 911215-020341	8605	02:01	C 3.5	2087	1175	533	†	†	1.53 E+04	25.1
sf 911215-113305	8605	11:38	C 8.6	2096	1178	658	†	†	1.98 E+05	24.6
sf 911215-183201	8605	18:29	M 1.4	2102	1181	483	†	†	4.89 E+05	23.9
sf 911220-135723	8610	14:00	X 3.5	2174	1199	800	2706	169	1.20 E+06	11.7
sf 920126-145023	8647	14:32	C 5.3	2511	1316	300	438	36	1.75 E+03	6.8
sf 920202-090451	8654	08:59	M 2.3	2551	1336	500	214	68	1.13 E+05	14.0
sf 920202-224407	8654	22.46	M 1.3	3088	1340	500	853	68	1.82 E+04	17.5
sf 920204-075349	8656	07:41	C 3.7	2596	1351	250	†	†	4.40 E+03	22.7

Notes: † Marginal detection.
∗ Detector saturation.

Table 10. Upper limits to galactic black hole candidates $|b| < 10°$

Source	Position		2σ Flux (10^{-5} cm^{-2} s^{-1})				Note	Ref.
	l [deg]	b [deg]	$(0.75-1)$ [MeV]	$(1-3)$ [MeV]	$(3-10)$ [MeV]	$(10-30)$ [MeV]		
GRO J1719−24	2.4	7.0	< 3.5	7.8 ± 2.6	< 2.2	< 0.78	a,b,c	(1)
			< 3.68	< 3.64	< 1.54	< 0.76	a,c	(2)
GRS 1758−258	4.5	−1.4	< 3.5	< 3.8	< 1.7	< 0.64	a,c	(1)
GRS 1826−238	9.3	−6.0	< 6.8	< 8.8	< 3.4	< 1.10	a,c	(1)
			< 7.2	< 3.6	< 2.97	< 1.22	a,c	(2)
EXO 1846−031	29.9	−0.9	< 5.0	< 3.2	< 2.8	< 0.88	a,c	(1)
			< 4.5	< 4.63	< 1.99	< 1.09	a,c	(2)
SS433	39.7	−2.2	< 4.3	< 3.0	< 2.8	< 0.78	a,c	(1)
			< 9.13	< 4.37	< 2.41	< 0.76	a,c	(2)
GRS 1915+105	45.3	−0.9	< 5.3	< 3.4	< 3.2	< 0.76	a,c	(1)
			5.70 ± 2.69	< 4.29	< 2.56	< 0.76	a,c	(2)
4U 1957+115	51.3	−9.30	< 2.8	< 9.8	3.6 ± 1.0	< 0.86	a,b,c	(1)
			< 4.05	< 8.17	< 3.66	< 0.96	a,c	(2)
GS 2000+251 (QZ Vul)	63.4	−3.1	< 2.8	< 3.4	< 3.5	< 0.66	a,c	(1)
			< 4.55	< 4.38	< 2.14	< 0.63	a,c	(2)
GS 2023+338 (V 404)	73.2	−2.2	< 6.3	< 6.8	< 2.6	< 0.54	a,c	(1)
			10.25 ± 3.03	8.95 ± 2.50	< 2.33	< 0.58	a,b,c	(2)
WR 148	90.08	6.47	< 4.60	< 9.87	< 2.71	< 0.65	a,c	(2)
A 0620−00 (Nova Mon 1975)	210.0	−6.5	< 3.5	< 3.8	< 2.4	< 0.98	a,c	(1)
			< 5.46	< 5.38	< 3.17	< 1.51	a,c	(2)
GRS 1009−45	275.9	9.4	< 7.0	< 5.6	< 3.6	< 1.06	a,c	(1)
(Nova Vel 1993)			< 11.69	< 5.52	< 1.94	< 0.93	a,c	(2)
GRS 1124−684 (Nova Mus 1991)	295.0	−7.1	< 6.8	< 3.4	< 4.7	< 1.28	a,c	(1)
			< 4.4	< 4.55	< 2.05	< 1.32	a,c	(2)

Table 10. continued

Source	Position		2σ Flux (10^{-5} cm^{-2} s^{-1})				Note	Ref.
GS 1354−645	310.0	−2.8	< 9.8 < 10.2	< 6.8 < 7.89	< 2.7 < 4.61	< 2.00 < 1.17	a,c a,c	(1) (2)
	l [deg]	b [deg]	$(0.75-1)$ [MeV]	$(1-3)$ [MeV]	$(3-10)$ [MeV]	$(10-30)$ [MeV]		
TrA X−1 (A1524−617)	320.32	−4.43	8.58 ± 3.80 < 7.3	< 12.97 < 8.2	< 3.17 < 2.8	< 2.60 < 2.80	a,b,c a,c	(2) (1)
4U 1543−475	330.9	5.4	< 6.0 < 7.45	< 4.2 < 8.97	< 1.7 < 2.23	< 0.74 < 0.96	a,c a,c	(1) (2)
4U 1630−472	336.9	0.3	< 3.3 < 3.93	< 3.4 < 4.22	< 1.8 < 1.96	< 1.20 < 1.03	a,c a,c	(1) (2)
GX 339−4	338.9	−4.3	< 0.35 < 5.48	< 3.6 < 7.75	< 1.8 < 2.60	< 0.74 < 0.78	a,c a,c	(1) (2)
GRO J1655−40 (Nova Sco 1994)	344.9	2.5	< 3.8 < 7.07	< 3.8 < 5.42	< 1.7 < 1.73	< 1.16 < 0.99	a,c a,c	(1) (2)
H 1741−322	357.1	−1.6	< 4.0 < 3.68	< 4.2 < 6.68	< 2.0 < 2.26	< 0.72 < 0.60	a,c a,c	(1) (2)
4U 1755−338 (Nova Oph 1977)	357.2	−4.9	< 4.0 < 3.67	< 4.97	< 2.0 < 2.17	< 0.72 < 0.60	a,c a,c	(1) (2)
H 1705−250	358.6	9.1	< 4.0 < 4.93	< 4.2 < 6.09	< 2.0 < 1.58	< 0.86 < 0.60	a,c a,c	(1) (2)
GRS 1734−292	358.84	1.40	< 3.68	< 5.69	< 1.53	< 1.25	a,c	(2)
1E 1740.7−2942	359.1	−0.1	< 4.0 < 3.67	< 4.2 < 5.53	< 2.0 < 2.17	< 1.66 0.93 ± 0.36	a,c a,b,c	(1) (2)

Notes

(a) Model for diffuse galactic emission included in analysis.
(b) A positive flux measurement does not necessarily indicate a source detection (see Ref. 1).
(c) All upper limit fluxes are applied to data from Phases I to III.

References

(1) McConnell et al. (1996)
(2) van Dijk (1996)

Table 11a. COMPTEL 2σ upper limits to AGN (EGRET sources and Seyferts)

Name	Location				Upper limit (10^{-5} cm^{-2} s^{-1})				Type	Other name
	RA [deg]	DEC [deg]	l [deg]	b [deg]	$(0.75-1.0)$ [MeV]	$(1-3)$ [MeV]	$(3-10)$ [MeV]	$(10-30)$ [MeV]		
0003+199	1.59	20.21	108.77	−41.42	< 4.24	< 4.92	< 5.03	< 0.90	SY	MRK 335
0007+107	2.63	10.97	106.98	−50.63	< 3.70	< 5.12	< 2.46	< 0.89	SY	IIIZW2
0121−590	20.94	−58.81	295.08	−57.82	< 4.67	< 7.72	< 2.14	< 0.84	SY	FAIRALL 9
0130−171	23.18	−16.91	168.12	−76.02	< 6.60	< 7.70	< 7.84	< 1.52	2 EG	
0202+149	31.21	15.24	147.93	−44.04	< 8.57	< 10.56	< 2.51	< 0.90	2 EG	
0208−512	32.69	−51.02	276.10	−61.78	< 8.98	< 12.94	< 2.97	< 1.76	2 EG	
0219+428	35.66	43.03	140.14	−16.77	< 2.95	< 3.74	< 2.17	< 0.80	2 EG	
0234+285	39.47	28.80	149.47	−28.53	< 2.94	< 3.78	< 1.90	< 0.76	2 EG	
0235+164	39.66	16.62	156.77	−39.11	< 3.03	< 6.24	< 3.70	< 1.20	2 EG	
0240−002	40.67	−0.01	172.11	−51.93	< 7.15	< 8.64	< 2.84	< 1.19	SY	NGC 1068
0420−014	65.82	−1.34	195.29	−33.14	< 3.33	< 4.38	< 2.59	< 1.11	2 EG	
0430+052	68.29	5.35	190.37	−27.40	< 3.74	< 6.42	< 2.62	< 0.98	SY	3C 120
0440−003	70.66	−0.30	197.20	−28.46	< 2.59	< 4.00	< 1.83	< 0.94	2 EGS	
0446+112	72.28	11.35	187.43	−20.74	< 2.67	<3.42	<1.68	< 0.65	2 EG	
0454−463	73.97	−46.27	251.97	−38.81	< 2.98	< 4.08	< 5.97	< 0.88	1 EG	
0454−234	74.26	−23.42	223.71	−34.90	< 2.95	< 9.08	< 2.39	< 1.19	1 EG	
0458−020	75.30	−1.99	201.45	−25.30	< 2.57	< 3.60	< 1.97	< 0.68	2 EG	
0513−002	79.05	−0.15	201.69	−21.13	< 2.50	< 3.42	< 2.27	< 0.61	SY	ARK 120
0521−365	80.74	−36.46	240.61	−32.72	< 4.03	< 5.40	< 2.66	< 1.03	2 EG	
0528+134	82.74	13.53	191.37	−11.01	< 6.79	13.44	5.02	< 1.46	2 EG	
0537−441	84.71	−44.08	250.08	−31.09	< 5.32	< 6.05	< 2.07	< 1.02	2 EG	
0551+464	88.73	46.44	165.73	10.41	< 2.34	< 3.16	< 1.67	< 0.65	SY	MCG+8-11-11
0716+714	110.48	71.34	143.98	28.02	< 2.87	< 3.60	< 3.72	< 0.68	2 EG	
0735+178	114.53	17.70	201.85	18.07	< 1.56	< 3.21	< 1.20	< 1.05	2 EG	
0805−077	122.06	−7.85	229.04	13.16	< 11.57	< 16.50	< 3.85	< 1.59	2 EG	
0804+499	122.16	49.85	169.16	32.56	< 2.16	< 2.63	< 1.04	< 1.95	2 EG	
0827+243	127.71	24.18	200.02	31.87	< 1.92	< 1.97	< 1.05	< 1.10	2 EG	
0829+046	127.95	4.50	220.69	24.33	< 2.13	< 2.98	< 3.52	< 1.56	2 EG	
0836+710	130.36	70.89	143.54	34.43	< 2.89	< 3.55	< 2.39	< 0.66	2 EG	
0917+449	140.25	44.70	175.70	44.82	< 3.04	2.30	< 0.87	< 1.16	2 EG	
0931+275	143.57	27.33	200.83	46.47	< 1.68	< 1.89	< 0.94	< 0.85	SY	MCG+5-23-16
0954+556	149.41	55.38	158.60	47.93	< 1.39	< 4.84	< 0.99	< 0.62	2 EG	
0954+658	149.69	65.56	145.75	43.13	< 2.70	< 3.35	< 1.94	< 0.62	2 EG	
1020+201	155.88	19.84	217.03	55.44	< 1.70	< 2.89	< 1.18	< 0.90	SY	NGC 3227
1101+384	166.11	38.21	179.83	65.03	< 2.50	< 4.58	< 0.98	< 0.69	2 EG	MRK 421
1127−145	172.53	−14.82	275.28	43.64	< 2.61	< 3.66	< 7.73	0.82	2 EG	
1136−374	174.76	−37.74	287.46	22.95	< 3.41	< 7.22	< 2.49	< 1.44	SY	NGC 3783
1156+295	179.89	29.24	199.42	78.38	< 2.42	< 3.17	< 4.80	0.80	2 EG	
1200+448	180.79	44.54	148.88	70.08	< 2.56	< 3.49	< 1.95	< 1.04	SY	NGC 4051
1208+396	182.63	39.41	155.08	75.06	< 2.88	< 3.85	< 2.13	1.11	SY	NGC 4151
1219+285	185.38	28.23	201.74	83.29	< 2.30	< 3.09	< 2.34	< 0.84	1 EG	
1219+285	185.38	28.23	201.74	83.29	< 2.30	< 3.09	< 2.34	< 0.84	2 EGS	
1226+023	187.28	2.05	289.95	64.36	< 2.41	9.66	5.19	< 0.89	2 EG	3C 273

Table 11a. continued

Name	Location				Upper limit (10^{-5} cm^{-2} s^{-1})				Type	Other name
	RA [deg]	DEC [deg]	l [deg]	b [deg]	(0.75 − 1.0) [MeV]	(1 − 3) [MeV]	(3 − 10) [MeV]	(10 − 30) [MeV]		
1229−021	188.00	−2.40	293.16	60.10	< 2.38	< 5.56	< 3.84	< 0.74	2 EG	
1237−050	189.92	−5.35	297.49	57.40	< 2.50	< 3.07	< 1.98	< 0.95	SY	NGC 4593
1253−055	194.04	−5.79	305.10	57.06	< 3.23	< 6.64	< 2.91	< 0.97	2 EG	3C 279
1313−333	199.03	−33.65	308.80	28.94	< 2.80	< 3.48	< 2.38	< 0.70	2 EG	
1317+520	199.94	51.80	112.63	64.76	< 2.92	< 4.04	< 2.18	< 1.27	2 EG	
1322−428	201.37	−43.02	309.52	19.42	< 5.60	< 12.04	< 3.87	< 0.84	2 EG	CEN A
1331+170	203.40	16.82	348.51	75.81	< 4.57	< 3.91	< 2.26	< 0.68	2 EG	
1333−340	203.96	−34.29	313.28	27.69	< 2.54	< 3.45	< 1.79	< 0.71	SY	MCG-6-30-15
1346−300	207.32	−30.31	317.49	30.92	< 2.71	< 3.65	< 1.76	< 0.70	SY	IC4329A
1460−076	212.24	−7.88	333.88	50.28	< 4.48	< 7.51	< 1.74	< 0.68	2 EG	
1410−029	213.31	−3.21	339.15	53.81	< 3.80	< 10.68	< 1.69	< 0.69	SY	NGC 5506
1415−253	214.49	25.14	31.96	70.50	< 6.36	< 14.14	< 4.49	< 1.20	SY	NGC 5548
1424−418	216.99	−42.10	321.45	17.27	< 3.22	< 3.44	< 3.39	< 0.98	2 EGS	
1510−089	228.21	−9.10	351.29	40.14	< 6.63	< 10.74	< 4.41	< 1.29	2 EG	
1517+656	229.46	65.43	102.26	45.38	< 4.68	< 7.21	< 10.07	< 4.13	O	
1604+159	241.78	15.86	29.38	43.41	< 4.02	< 16.26	< 8.21	< 1.81	2 EG	
1606+106	242.19	10.49	23.03	40.79	< 3.99	< 6.53	< 6.43	1.55	2 EG	
1611+343	243.42	34.21	55.15	46.38	< 5.70	< 6.28	3.21	< 1.46	2 EG	
1622−253	246.44	−25.46	352.14	16.32	< 2.23	< 3.02	< 1.58	< 0.70	2 EG	
1622−297	246.52	−29.85	348.82	13.32	< 2.44	< 3.12	< 1.62	< 0.83	2 EG	
1633+382	248.81	38.14	61.09	42.34	< 5.45	< 6.56	< 6.78	< 2.16	2 EG	
1730−130	263.26	−13.08	12.30	10.81	< 2.07	< 6.00	< 2.35	< 0.66	2 EG	
1739+522	265.15	52.19	79.56	31.75	< 3.27	< 8.74	< 4.65	0.99	2 EG	
1741−038	265.99	−3.83	21.59	13.13	< 4.01	< 4.19	< 5.43	< 0.76	1 EG	
1908−201	287.79	−20.12	16.87	−13.22	< 2.13	< 2.90	< 2.63	< 1.08	2 EG	
1916−587	290.31	−58.67	338.18	−26.71	< 3.42	< 5.00	< 3.00	< 1.04	SY	ESO 141 − 55
1933−400	294.32	−39.97	359.16	−25.37	< 2.83	< 3.34	< 1.74	< 0.84	2 EG	
1939−104	295.67	−10.32	29.35	−16.01	< 5.43	< 3.62	< 2.27	< 0.79	SY	NGC 6814
2005−489	302.35	−48.83	350.37	−32.60	< 3.74	< 4.96	< 2.49	< 0.97	1 EG	
2022−077	306.41	−7.59	36.90	−24.38	< 3.28	< 4.44	< 2.38	< 1.04	2 EG	
2041−109	311.04	−10.73	35.97	−29.86	< 5.07	< 6.56	< 2.52	< 1.08	SY	MRK 509
2052−474	314.07	−47.25	352.59	−40.38	< 4.42	< 5.84	< 2.93	< 1.03	2 EG	
2155−304	329.72	−30.23	17.73	−52.25	< 5.37	< 5.36	< 2.93	< 1.35	O	
2209+236	333.02	23.92	82.24	−26.09	< 2.43	< 3.50	< 3.53	< 0.72	2 EG	
2221−023	335.95	−2.10	61.86	−46.71	< 4.47	< 5.04	< 2.34	< 0.90	SY	3C 445
2230+114	338.15	11.73	77.44	−38.58	< 3.36	< 8.06	< 2.96	< 0.98	2 EG	CTA 102
2233−263	338.94	−26.05	27.14	−59.74	< 3.89	< 5.48	< 5.74	< 1.34	SY	NGC 7314
2251+158	343.49	16.15	86.11	−38.18	< 4.37	< 9.28	< 6.63	< 1.53	2 EG	3C 454.3
2300+086	345.82	8.87	83.10	−45.47	< 3.52	< 6.98	< 4.25	< 1.17	SY	NGC 7469
2302−090	346.23	−8.73	64.08	−58.82	< 3.46	< 4.68	< 5.78	< 1.30	SY	MCG-2-58-22
2315−426	349.60	−42.37	348.08	−65.70	< 5.81	< 8.86	< 5.27	< 1.30	SY	NGC 7582
2356+196	359.69	19.92	106.38	−41.25	< 3.47	< 4.84	< 4.12	< 0.91	2 EG	

Table 11b. COMPTEL 2σ upper limits to unidentified high-latitude EGRET sources

Name	Location				Upper limit (10^{-5} cm^{-2} s^{-1})				Type
	RA [deg]	DEC [deg]	l [deg]	b [deg]	$(0.75-1.0)$ [MeV]	$(1-3)$ [MeV]	$(3-10)$ [MeV]	$(10-30)$ [MeV]	
2EG J0008+7307	2.09	73.13	119.77	10.52	< 5.29	< 4.48	< 2.18	< 1.01	2 EG
2EG J0119+0312	19.97	3.21	136.77	−58.90	< 4.63	< 5.36	< 8.43	< 1.03	2 EG
2EG J0159−3557	29.85	−35.95	248.55	−73.08	< 9.06	< 11.08	< 3.95	< 2.46	2 EG
2EG J0216+1107	34.00	11.12	153.93	−46.60	< 6.12	< 6.12	<4.51	< 0.94	2 EG
2EG J0403+3357	60.95	33.96	162.40	−13.79	< 3.23	< 3.25	< 1.61	< 0.72	2 EG
2EG J0406+1704	61.67	17.08	175.61	−25.23	< 2.38	< 3.26	< 2.01	< 0.69	2 EG
2EG J0422+1414	65.53	14.24	180.65	−24.26	< 2.24	< 3.10	< 2.04	< 0.66	2 EG
2EG J0426+6618	66.52	66.31	142.24	11.87	< 2.42	< 5.58	< 2.16	< 0.74	2 EG
2EGS J0426+1636	66.66	16.61	179.40	−21.92	< 2.31	< 3.10	< 1.93	< 0.66	2EGS
2EG J0432+2910	68.21	29.18	170.34	−12.68	< 2.34	< 2.98	< 1.48	< 0.60	2 EG
2EG J0437+1524	69.30	15.41	182.10	−20.68	< 2.36	< 3.06	< 1.57	< 0.64	2 EG
2EGS J0500+5902	75.15	59.04	150.50	10.26	< 3.38	< 5.59	< 1.97	< 0.69	2 EGS
2EG J0532−6914	83.24	−69.24	279.70	−32.16	< 2.78	< 4.51	< 2.98	< 0.66	2 EG
2EGS J0552−1026	88.12	−10.45	215.78	−17.78	< 2.54	< 3.76	< 2.38	< 0.67	2 EGS
2EGS J0555+0408	88.95	4.14	202.77	−10.40	< 2.49	< 3.29	< 1.84	< 0.59	2 EGS
2EG J0617−0652	94.42	−6.88	215.27	−10.62	< 2.42	< 3.52	< 4.91	< 0.84	2 EG
2EG J0720−4746	110.12	−47.78	259.24	−15.19	< 2.84	< 8.64	< 4.75	< 0.68	2 EG
2EGS J0724−5157	111.02	−51.97	263.47	−16.34	< 2.59	< 4.61	< 2.42	< 0.64	2 EGS
2EG J0744+5438	116.12	54.64	163.18	29.34	< 2.33	< 2.12	< 1.55	< 0.95	2 EG
2EG J0809+5117	122.27	51.29	167.46	32.74	< 1.96	< 2.14	< 1.05	< 1.97	2 EG
2EG J0852−1237	133.12	−12.63	239.35	19.75	< 9.25	< 21.56	< 3.93	< 1.39	2 EG
2EGS J0909+6558	137.43	65.97	148.29	38.47	< 2.74	< 3.42	< 1.61	< 0.64	2 EGS
2EGS J1050−7650	162.53	−76.85	296.08	−15.62	< 2.88	< 3.86	< 4.35	< 0.78	2 EGS
2EG J1054+5736	163.70	57.61	148.80	53.26	< 3.06	< 3.58	< 1.38	0.60	2 EG
2EGS J1133+0037	173.33	0.63	264.41	57.54	< 2.48	< 3.32	< 2.35	< 1.01	2 EGS
2EG J1136−0414	174.23	−4.24	270.26	53.84	< 2.52	< 3.32	< 1.68	< 0.66	2 EG
2EG J1220−1510	185.00	−15.17	291.77	47.02	< 3.76	< 2.90	< 5.12	< 1.53	2 EGS
2EG J1233−1407	188.27	−14.13	296.20	48.50	< 4.94	< 2.80	< 4.19	< 0.72	2 EG
2EGS J1236−0416	189.00	−4.27	295.58	58.38	< 2.28	< 3.73	< 2.41	< 0.90	2 EGS
2EG J1239+0441	189.82	4.69	295.04	67.38	< 2.59	9.24	< 4.38	< 1.14	2 EG
2EG J1248−8308	192.06	−83.14	302.83	−20.27	< 2.89	< 4.04	< 2.65	< 0.88	2 EG
2EGS J1324+2210	201.20	22.18	1.59	80.95	< 2.26	< 3.07	< 3.63	< 0.68	2 EGS
2EG J1332+8821	203.03	88.35	122.60	28.75	< 4.98	< 3.99	< 2.03	< 0.83	2 EG
2EG J1346+2942	206.70	29.70	48.11	77.57	< 2.79	< 8.00	< 2.40	< 1.06	2 EG
2EG J1430+5356	217.66	53.95	95.52	57.58	< 3.91	< 8.72	< 6.21	< 1.42	2 EG
2EG J1457−1916	224.36	−19.27	339.68	34.46	< 2.92	< 8.78	< 2.10	< 0.88	2 EG
2EGS J1504−1537	226.22	−15.63	344.06	36.37	< 5.01	< 9.66	< 2.23	< 0.92	2 EGS
2EG J1528−2352	232.15	−23.87	343.23	26.45	< 2.33	< 3.45	< 3.00	< 0.84	2 EG
2EG J1631−2845	247.76	−28.75	350.40	13.26	< 2.37	< 3.00	< 1.57	< 0.78	2 EG
2EG J1635−1427	248.76	−14.46	2.57	21.67	< 2.28	< 3.23	< 1.67	< 0.72	2 EG
2EGS J1642−2659	250.62	−26.99	353.46	12.48	< 2.96	< 2.97	< 1.51	< 0.92	2 EGS
2EGS J1703−6302	255.79	−63.05	327.39	−12.88	< 3.22	< 4.52	< 2.38	< 1.20	2 EGS
2EGS J1708−0927	257.16	−9.47	11.92	17.80	< 2.25	< 3.11	< 3.88	< 0.68	2 EGS
2EG J1709−0350	257.32	−3.84	17.07	20.63	< 2.43	< 3.29	< 4.76	< 0.80	2 EG
2EG J1731+6007	262.90	60.12	88.93	33.14	< 5.09	< 9.06	< 3.17	< 1.16	2 EG
2EG J1815+2950	273.83	29.84	56.89	20.37	< 2.74	< 3.70	< 2.83	< 2.09	2 EG
2EG J1821−7915	275.43	−79.26	314.72	−25.25	< 3.78	< 5.12	< 5.59	< 1.06	2 EG
2EG J1835+5919	278.78	59.33	88.74	25.12	< 3.12	< 8.64	< 2.13	< 1.28	2 EG
2EGJ 1847−3220	281.84	−32.35	3.17	−13.33	< 2.14	< 2.86	< 1.43	< 0.62	2 EG
2EG J1850−2638	282.74	−26.65	8.82	−11.70	< 3.90	< 2.91	< 2.68	< 0.62	2 EG
2EG J1950−3503	297.51	−35.06	5.17	−26.50	< 5.16	< 3.38	< 1.72	< 0.74	2 EG
2EGS J1954−1419	298.75	−14.33	26.85	−20.42	< 2.62	< 3.50	< 2.97	< 1.57	2 EGS
2EG J2006−2253	301.62	−22.90	19.32	−26.17	< 2.95	< 3.68	< 3.88	< 0.77	2 EG
2EG J2027+1054	306.79	10.91	54.24	−15.55	< 2.39	< 8.02	< 4.73	< 1.01	2 EG
2EG J2243+1545	340.82	15.75	83.17	−37.04	< 3.89	< 7.42	< 4.96	< 1.64	2 EG
2EGS J2322−0321	350.60	−3.36	77.24	−58.10	< 3.68	< 4.76	< 3.27	< 1.27	2 EGS
2EG J2354+3811	358.56	38.19	110.73	−23.32	< 4.41	< 5.41	< 3.42	< 0.93	2 EG

Table 12. Upper limits to possible sources of gamma-ray line emission

Name	Position l [deg]	Position b [deg]	Line Energy [MeV]	Flux (2 σ) [10^{-5} photons cm^{-2} s^{-1}]	Observation Period	Note	Ref.
SN 1993J	142.15°	40.92°	0.847 1.238	< 6.2 < 2.9	VP 227.0, 228.0, 319.0, 319,0, 319.5	(a)	(2)
Kepler SN (1604)	4.52	+6.84	1.157	< 1.43	Phases I to III		(1)
Tycho SN (1572)	120.09	+1.42	1.157	< 1.78	Phases I to III		(1)
3C 58	130.72	+3.08	1.157	< 1.78	Phases I to III		(1)
Lupus SN (1006)	327.51	+14.69	1.157	< 1.50	Phases I to III		(1)
Novae (general)			1.275 MeV	< 3	April 1991–Aug 1993		(4)
Nova Cen 1991	309°	−1.04°	1.275	< 4.0	VP 12.0, 14.0, 23.0, 27.0, 208.0, 215,0, 217.0, 314.0, 315.0, 316.0	(b)	(4)
Nova Her 1991	43.3°	6.6°	1.275 MeV	< 3.3	VP 20.0, 328.0, 331.x, 333.0	(b)	(4)
Nova SGR 1991	0.18°	−6.94°	1.275	< 6.2	5.0, 210.0, 214.0, 219.4, 223.0, 226.0, 231.0, 229.x, 232.x, 302.3, 223.0, 324.0, 330.0, 332.0, 334.0, 336.5, 338.0	(b)	(4)
Nova Sct 1991	25.1°	−2.80°	1.275	< 3.6	7.5, 13.0, 20.0, 231.0, 229.x, 324.0, 330.0, 332.0, 334.0	(b)	(4)
Nova Pup 1991	252.7°	−0.72°	1.275	< 5.5	41.0, 44.0, 230.0, 301.0, 338.5	(b)	(4)
Nova Cyg 1992	89.14°	7.82°	1.275	< 2.3	34.0, 203.x, 212.0, 302.x, 318.1	(b)	(4)
Nova Sco 1992	343.8°	−1.61°	1.275	< 5.9	27.0, 210.0, 214.0, 219.4, 223.0, 226.0 229.x, 232.x, 302.3 323.0, 336.5, 338.0	(b)	(4)
Nova Sgr 1992−1	4.75°	−2.0°	1.275	< 6.0	210.0, 214.0, 219.4, 223.0, 226.0, 231.0, 229.x, 232.0, 302.3, 323.0, 324.0, 330.0, 332.0, 334.0, 336.5, 338.0	(b)	(4)

Table 12. continued

Name	Position l [deg]	Position b [deg]	Line Energy [MeV]	Flux (2 σ) [10^{-5} photons cm^{-2} s^{-1}]	Observation Period	Note	Ref.
Nova Sgr 1992−2	4.56°	−6.96°	1.275	< 3.0	214.0, 223.0, 226.0, 231.0, 229.x, 232.x, 302.3, 323.0, 324.0, 330.0, 332.0, 334.0, 334.0, 338.0	(b)	(4)
Nova Sgr 1992−3	9.38°	−4.54°	1.275	< 4.4	210.0, 214.0, 219.4, 223.0, 226.0, 231.0, 229.x, 232.x, 302.3, 323.0, 324.0, 330.0, 332.0, 334.0	(b)	(4)
Nova Aql 1993	36.81°	−4.10°	1.275	< 6.2	231.0, 324.0, 330.0, 332.0	(b)	(4)
Cygnus Loop	74.01	−8.56	1.809	< 1.50	Phases I to III	(c)	(6)
HB 21	88.86	4.80	1.809	< 2.30	Phases I to III	(d)	(6)
Mon Nebula	204.96	0.45	1.809	< 1.60	Phases I to III	(c)	(6)
Lupus Loop	329.67	15.97	1.809	< 1.40	Phases I to III	(e)	(6)
Orion	209.0°	−19.4°	1.809	< 1.7	VP 1.0 VP 2.5 (solar mode) VP 221.0 VP 337.0		(3)
Cyg X−1	71.3	+3.1	2.223	< 1.53	VP 1 − 523		(5)
Sco X−1	359.09	23.78	2.223	< 1.7	Phases I to IV / Cycle-5		(5)
Cyg X−3	79.85	0.70	2.223	< 1.2	Phases I to IV / Cycle-5		(5)
4U 1916−05	31.38	−8.22	2.223	< 1.2	Phases I to IV / Cycle-5		(5)
4U 1626−67	321.79	−13.09	2.223	< 1.7	Phases I to IV / Cycle-5		(5)
4U 1820−30	2.79	−7.91	2.223	< 1.1	Phases I to IV / Cycle-5		(5)

References
(1) Dupraz et al. (1997)
(2) Lichti et al. (1996)
(3) Oberlack et al. (1995)
(4) Iyudin et al. (1995)
(5) McConnell et al. (1997b)
(6) Knödlseder et al. (1996)

(a) Only VP 227/228 used for upper flux limit.
(b) Only observations up to VP 232 used for upper flux limit.
(c) radius 2°.
(d) radius 1°.
(e) radius 1.5°.

Table 13. Summary of most significant COMPTEL source detections

Type of Source	Number of Sources	Comments
Spin-Down Pulsars:	3	Crab, Vela, PSR B1509−58.
Stellar Black Hole Candidates:	2	Cyg X−1, Nova Persei 1992 (GRO J0422+32).
Supernova Remnants: (Continuum Emission)	1	Crab nebula.
Active Galactic Nuclei:	10	CTA 102, 3C 454.3, PKS 0528+134, GRO J 0516−609, PKS 0208−512, 3C 273, PKS 1222+216, 3C 279, Cen A, PKS 1622−297.
Unidentified Sources:		
• $\|b\| < 10^\circ$	4	GRO J1823−12, GRO J2228+61 (2CG 106+1.5), GRO J0241+6119 (2CG 135+01), Carina/Vela region (extended).
• $\|b\| > 10^\circ$	5	GRO J1753+57 (extended), GRO J1040+48, GRO J1214+06, HVC complexes M and A area (extended), HVC complex C (extended).
Gamma-Ray Line Sources:		
• 1.809 MeV (^{26}Al)	3	Cygnus region (extended), Vela region (extended, may include RX J0852−4621), Carina region.
• 1.157 MeV (^{44}Ti)	2	Cas A, RX J0852−4621 (GRO J0852−4642).
• 0847 and 1.238 MeV (^{56}Co)	1	SN 1991T.
• 2.223 MeV (n-capture)	1	GRO J0317−853.
Gamma-Ray Burst Sources: (within COMPTEL field-of- up to Phase IV/Cycle-5)	31	Location error radii vary from 0.34° to 2.79° (mean error radius: view 1.13°).